Impedance Modeling and Stability Analysis of Grid-Interactive Converters

Liao, Yicheng

DOI (link to publication from Publisher):
10.5278/vbn.phd.eng.00086

Publication date:
2020

Document Version
Publisher's PDF, also known as Version of record

IMPEDANCE MODELING AND STABILITY ANALYSIS OF GRID-INTERACTIVE CONVERTERS

BY
YICHENG LIAO

DISSERTATION SUBMITTED 2020

AALBORG UNIVERSITY
DENMARK

IMPEDANCE MODELING AND STABILITY ANALYSIS OF GRID-INTERACTIVE CONVERTERS

by

Yicheng Liao

AALBORG UNIVERSITY
DENMARK

Dissertation submitted

.

Dissertation submitted: December 2020

PhD supervisor: Prof. Xiongfei Wang,
Aalborg University

PhD committee: Professor Birgitte Bak-Jensen (chairman)
Aalborg University

Professor Alex M. Stankovic
Tufts University

Professor Marta Molinas
Norwegian University of Science and Technology

PhD Series: Faculty of Engineering and Science, Aalborg University

Department: Department of Energy Technology

ISSN (online): 2446-1636
ISBN (online): 978-87-7210-865-0

Published by:
Aalborg University Press
Kroghstræde 3
DK – 9220 Aalborg Ø
Phone: +45 99407140
aauf@forlag.aau.dk
forlag.aau.dk

Printed in Denmark by Rosendahls, 2021

ENGLISH SUMMARY

As the increased penetration of renewable generation sources, more power electronic converters are connected to the modern electric power grids. Their fast switching and flexible control dynamics tend to result in instability issues to the power system. To deal with this topic holistically, this PhD thesis focuses on the development of impedance-based modeling and stability analysis approaches for converter-based systems and the application of these methods for converter control design.

The converter systems are nonlinear and time periodic, whose impedance models can be derived based on linearization and frequency-domain modelling. The unified frequency-domain modelling and validation approaches for three-phase grid-interactive converters under both balanced and unbalanced conditions are developed. First, the stationary-frame impedance modeling and measurement methods of grid-interactive converters in three-phase balanced grids are proposed. Then, the modeling approach is generalized to the three-phase unbalanced grids considering more frequency coupling dynamics brought by the unbalanced voltage trajectory.

An interconnected converter system can be modeled as a closed-loop feedback system using impedance models, based on which the system stability can be further analyzed in the frequency domain. The converter impedances can be characterized as single-input single-output (SISO) or multi-input multi-output (MIMO) models considering different control-loop dynamics. A general impedance-based stability analysis approach is proposed first for SISO systems based on the Nyquist stability criterion (NSC), which enables to identify the open-loop right-half-plane poles directly from individual impedance Bode diagrams and to implement the impedance specification. Then, how to extend the SISO-based analysis to MIMO systems is introduced, based on the generalized NSC or the characteristic equation analysis.

The developed impedance modeling and stability analysis approaches are further applied to grid-forming converters for harmonic stability analysis and control design. The high-frequency harmonic instability issues caused by the voltage control of grid-forming converters in grid-connected applications are studied first based on the impedance passivity analysis. A passivity-based controller co-design approach is proposed to achieve the impedance passivity till half of the sampling frequency for stability enhancement. Then, the low-frequency instability of grid-forming converters in stiff grids considering the outer-loop control dynamics is studied. Based on the small-gain theorem and the impedance decomposition, different control-loop impacts on stability of grid-forming converters are further investigated, which can be used as guidelines for control parameter tuning for stability enhancement.

.

DANSK RESUME

I takt med indfasning af flere vedvarende energikilder, øges antallet af effektelektroniske konvertere i el-nettet. Effektelektronikkens hurtige skiftetider og fleksible kontrol-dynamikker kan resultere i ustabilitetsproblemer i nettet. For at belyse denne problemstilling, fokuserer PhD-afhandlingen på udvikling af en impedans-baseret modellering og stabilitets-analyse for effektelektroniske konverter-systemer og anvendelse af disse metoder i systemernes regulerings-design.

De effektelektroniske systemer er ikke-lineære og tidsperiodiske, således at modellering af deres impedans ofte baseres på linearisering og frekvensdomænet. En samlet modellering i frekvensdomænet og tilhørende validerings-metoder er udviklet for net-tilsluttede tre-fase effektelektroniske konvertere under både balanceret og ubalancerede net-forhold. Først præsenteres impedans-modellering med stationær reference og dertilhørende målemetoder af net-tilsluttede effektelektroniske systemer under balanceret operation. Dernæst generaliseres modellerings-tilgangen for ubalancerede tre-fase systemer, og herunder dynamikken ved kobling af flere frekvenser grundet en ubalanceret spændings-vektor.

Et sammenkoblet effektelektronisk konverter system kan modelleres som et lukket-sløjfe reguleringssystem ved brug af de udviklede impedans-modeller, hvorefter systemets stabilitet kan analyseres i frekvensdomænet. Systemets impedanser kan karakteriseres som enten single-input single-output (SISO) eller multiple-input multiple-output (MIMO) afhængig af forskellige kontrol-sløjfe dynamikker. I PhD-afhandlingen præsenteres en generel impedans-baseret stabilitetsanalyse for SISO-systemer baseret på Nyquists stabilitetskriterie, der muliggør at identificere åben-sløjfe polerne i det højre halvplan direkte fra de individuelle impedans Bode-diagrammer. Dernæst introduceres en metode til at udvide fra SISO-baseret analyse til MIMO-systemer, baseret på det generelle Nyquist-stabilitetskriterie og analyse af den karakteristiske ligning.

De udviklede metoder til impedans-modellering og stabilitetsanalyse, anvendes herefter på net-tilsluttede effektelektroniske konverter-systemer for harmonisk stabilitetsanalyse og regulerings-design. Problemstillingen med højfrekvent harmonisk ustabilitet forårsaget af spændings-regulering af de net-tilsluttede effektelektroniske konvertere studeres først ved impedans passivitets-analyse. Et passivitets-baseret regulator-design er præsenteret, der kan opnå impedans-passivitet op til halvdelen af sampling-frekvensen. Herefter undersøges lavfrekvens ustabilitet for konvertere tilsluttet stærke net, ved at betragte regulerings-dynamikken af den ydre sløjfe. Til slut undersøges forskellige regulerings-sløjfers indflydelse på stabiliteten af net-tilsluttede effektelektroniske konvertere, baseret på ”small-gain”-sætningen og dekomposition af impedansen, hvilket kan bruges som retningslinjer for justering af regulerings-parametre til at øge stabiliteten.

ACKNOWLEDGEMENTS

At the final stage of my PhD study, I would like thank the individuals and organizations for their assistances and supports in developing myself as an independent researcher and finishing this PhD thesis.

My greatest gratitude goes to my PhD supervisor, Prof. Xiongfei Wang. I benefit a lot from his enthusiasm and expertise in research, which inspire me to explore valuable research questions, develop critical thinking, and conduct meticulous researches. I also appreciate it much for his time and patience in countless discussions with me, even during his spare time in midnights and travels, as well as his encouragements when I felt upset about my research.

It is a great pleasure to work with Prof. Henrik Sandberg, who was the host supervisor of my study-abroad project in KTH Royal Institute of Technology, Sweden. I was impressed a lot by his active participation in and insightful suggestions on my research work.

I have spent a happy and fruitful time during my PhD study, thanks to all the colleagues and friends. I have to acknowledge the influential advises from Dr. Xiaolong Yue at the early stage of my PhD study, as well as those beneficial discussions with Prof. Dongsheng Yang, Dr. Donghua Pan and Dr. Heng Wu on my PhD topic. In addition, Dr. Zheming Jin, Dr. Dapeng Lu, Mr. Hong Gong and Mr. Shih-Feng Chou helped with my experiments in the lab, and other group members provided good suggestions during every project meeting and group meeting. Dr. Asger Bjørn Jørgensen helped me with the translation of this PhD thesis abstract into Danish. I would like to express my sincere gratitude to them.

I wish to thank all the collaborated researchers and experts for their time in technical discussions and their helpful comments, including Prof. Frede Blaabjerg and Dr. Mads Graungaard Taul with Aalborg University, Prof. Lennart Harnefors with KTH Royal Institute of Technology and Hitachi ABB Power Grids, Dr. Yunfeng Liu, Dr. Kai Xin, Dr. Fangcheng Liu with Huawei Watt Lab, Prof. Brendan McGrath, Mr. Haris Siraj and Mr. Ullah Nutkani with RMIT University.

I would like to thank my PhD assessment committee members, Prof. Birgitte Bak-Jensen with Aalborg University, Prof. Alex M. Stankovic with Tufts University, Prof. Marta Molinas with Norwegian University of Science and Technology, and all the anonymous reviewers of my papers, for their critical comments and instructive suggestions that assist me to improve my research.

During my PhD period, I was offered chances to visit the KEMA Labs (previously known as DNV GL) for doing experiments at the FLEX Power Grid Lab. Prof. Erik de Jong, Dr. Yin Sun and Mr. Andrew Burstein hosted me and offered great helps with the tests. My thanks go to them as well.

This PhD project has been funded by Aalborg University-Huawei Energy Innovation Center. I am indebted to all the related staffs in the Department of Energy Technology for their administrative works and all the experts from Huawei Watt Lab for their valuable comments on my work.

I would also like to express special thanks to my master supervisor, Prof. Zhigang Liu from Southwest Jiaotong University, China, for his support and encouragement in my pursuit of the PhD degree overseas.

Last but not least, I owe my deepest gratitude to my families for their endless love and support. Especially, I share the credit of my work with my husband, Hongbo Zhao. I could not fulfill my PhD study without his company and favors.

Yicheng

TABLE OF CONTENTS

TABLE OF FIGURES

CHAPTER 1. INTORDUCTION

"If you want to find the secrets of the universe, think in terms of energy, frequency and vibration."

— Nikola Tesla

1.1. BACKGROUND AND MOTIVATION

With more and more renewable energy sources (RESs) integrated to the modern power grid, such as wind farms and solar power plants, the Danish power system is going to achieve 100% green electricity by 2030. The RESs are distributed and intermittent. To provide efficient and reliable energy generation, power electronic converters, which are composed by switching power semiconductor devices, are widely used as electrical energy conversion interfaces for RESs [1]. With the replacement of traditional synchronous generators (SGs) by converter-based RESs, modern electrical power grid is moving towards a power-electronic-based power system [2], which is briefly named as *electronic power grid* in this thesis.

Differing from SGs, power converters can be controlled more flexibly and rapidly [3]. However, these benefits brought by converter controls also pose new challenges to the stability of electronic power grids. The converter control induces wide-timescale dynamics, which can interact with electrical power grids and result in various instability issues. Such instability problems are manifested with oscillations whose frequency may range from hertz to kilohertz [4]. It is thus of great significance to seek analytical approaches to the stability analysis of electronic power grids.

When power converters are connected to the grid, the converter control tend to interact with grid dynamics, resulting in small-signal stability problems [5]. The converter-based systems feature discontinuous, nonlinear and time-varying dynamics [6]. To analyze their small-signal dynamics, linearized modeling is required. Based on the linearized models, there are two major approaches to the stability analysis. One is the state-space analysis conducted in the time domain [7]. The other is the transfer-function-based analysis performed in the frequency domain, which is most widely developed as the impedance-based analysis [8] in recent years.

The state-space analysis derives the differential equations of state variables, based on which a linearized model can be deduced through linearization. Then the modal analysis and sensitivity analysis can be performed for stability assessment, by which the system oscillation modes can be identified and the state participation factors or parameter sensitivity can be studied [9]. However, the state-space model usually results in a high-order system due to the large number of state variables from both power circuits and control loops. And it requires the "white-box" modelling, since various converter control schemes may include different state variables, which need

to be known to establish the entire system differential equations. However, the detailed control schemes and parameters in converter systems are usually confidential, which brings difficulty to the state-space modelling.

The impedance-based modelling is developed in the frequency domain as transfer functions. The converter control dynamics can be characterized by an impedance model seen at the grid connection point, which is defined as the ratio of the voltage variables and current variables [10]-[12]. Then, the converter-grid interaction can be modelled as a feedback loop formed by converter impedance and grid impedance derived at the point of common connection, to which the Nyquist stability criterion (NSC) can be applied for stability assessment [13], [14]. Compared with the state-space model, the impedance model allows for the "black-box" modelling, since it characterizes the control dynamics through the input-output relationships using transfer functions. The transfer function models can be easily measured with the frequency scan [15]-[17], even without the knowledge of converter internal control schemes and parameters. Last but not the least, the impedance models can be analysed through Bode diagrams, which enables to visually understand converter-grid interactions in the frequency domain, such that a design-oriented analysis can be implemented for controller design [18], [19]. Considering these advantages, this PhD thesis mainly focuses on the impedance-based approaches to analysing converter-based systems.

1.2. STATE OF THE ART AND CHALLENGES

The impedance-based stability analysis can be studied from three aspects: a) how to derive the impedance models; b) how to analyse the system stability with impedance models; c) how to conduct the converter controller design for stability enhancement based on the impedance analysis.

1.2.1. MODELING

In recent years, there are a lot of research works focusing on the impedance modelling of grid-connected converters. Several impedance models for three-phase grid-connected converters have been developed.

The conventional way is to model the converter system in the synchronous reference (*dq*) frame. By transforming the reference frame from *abc* or $\alpha\beta$ frame into *dq* frame, the system can be modelled as a time-invariant one if the switching dynamics are neglected by the averaging operator [20], such that the linearization yields a linear time-invariant (LTI) system [21]. The derived averaged model is merely valid below half of the switching frequency. The *dq*-frame impedance model of a three-phase three-wire converter yields a two-by-two transfer function matrix under balanced grid conditions [11], [12]. Such a multiple-input multiple-output (MIMO) model representation is the consequence of asymmetrical *dq*-frame control dynamics brought

by the outer control loops. When only the inner loop control is considered, the system *dq*-frame dynamics become symmetrical, which enables to further derive the two-by-two impedance matrix model as a single-input single-output (SISO) impedance model using complex variables and complex transfer functions [22]. Such a SISO model can be used for stability analysis in a higher frequency range which is beyond the outer-loop control bandwidth.

Since all the input and output variables in the *dq* frame are time invariant, the derived *dq*-frame impedance model fails in revealing the frequency coupling dynamics in converter systems. In order to characterize the frequency coupling dynamics, the impedance model can be transformed into the complex *dq* frame [23]-[25]. Although the complex *dq*-frame variables are still time-invariant, the ac signals are represented by two complex *dq*-frame vectors rotating in opposite directions, such that the frequency couplings caused by asymmetrical control dynamics can be characterized [26].

However, the complex *dq*-frame representation still fails in characterizing the frequency couplings observed in the measured voltage and current in the stationary reference ($\alpha\beta$) frame. This motivates to further derive the model in the $\alpha\beta$ frame by applying an inverse *dq* transformation [27]. Some other methods that directly linearize the converter systems in the $\alpha\beta$ frame around the steady-state operating trajectories are also developed, e.g. the harmonic linearization [28] and the harmonic state-space (HSS) modelling for linear time-periodic (LTP) systems [29], [30]. The direct linearization in the $\alpha\beta$ frame is also used with modular multi-level converters to characterize couplings of more harmonic components [31].

There have been some discussions regarding the relationships of different impedance models [27], [32], yet these well-discussed models are only applicable for three-phase converters in balanced grid conditions. How to model the converter impedances under unbalanced grid conditions has not been explicitly figured out. One recent study has applied the HSS modelling to the converter system under unbalanced grid conditions [33]. However, this work merely derives an equivalent converter impedance model that takes the grid-impedance interaction into account. Thus, the resultant model is not the actual impedance model of the converter at its point of connection, which is thus less applicable when the converter is interconnected to systems of different types.

Considering the above state-of-the-art, two major research gaps for the modelling of converter-based systems can be identified:

- The existing $\alpha\beta$-frame models are mainly validated by stability analysis compared with time-domain validations. *How to implement the frequency-domain model validation (i.e., impedance measurement) for three-phase converters in the αβ frame is still unclear.*

- There is still lack of impedance modelling for three-phase converters in unbalanced grid conditions. This motivates us to further investigate *how the well-developed dq-frame or αβ-frame models can be generalized to three-phase unbalanced grid conditions*.

1.2.2. STABILITY ANALYSIS

Based on the impedance models, the stability of the converter-based system can be analysed by the frequency-domain tools. The basic idea is to apply the Nyquist stability criterion (NSC) to the impedance ratio of the interconnected converter system [13], [14]. If the impedance models are MIMO systems, the generalized NSC [35] can be utilized.

Since the impedance ratio can be seen as an open-loop gain of the interconnected system, the system stability should be judged based on the number of right-half-plane (RHP) poles and the number of encirclements of the Nyquist curve around the critical point [36]. The number of RHP poles can be resulted in the impedance ratio, which affect the stability analysis result [37]. Therefore, how to define the impedance ratio is important to stability analysis. It has been suggested to partition the system into two parts based on the source types [38], [39] (Type-Z system with a stable control output impedance and Type-Y system with a stable control output admittance). Then, the impedance ratio can be defined as the Type-Z system's impedance divided by the Type-Y system's impedance, such that there are no open-loop RHP poles in the impedance ratio. Then, the stability is satisfied if there is no encirclement of the Nyquist curve around the critical point. Such a "no encirclement" condition for the impedance ratio can be mapped to Bode diagrams of individual impedances to implement the impedance specification [40].

However, such a definition of impedance ratio may fail in the stability prediction in a system with cascaded voltage sources, which are both Type-Z systems [41]. These systems may have RHP zeros in their impedances, such that the RHP poles can still be produced in the impedance ratio. In such cases, the impedance sum criterion can be used instead, which is based on analysing the entire system's characteristic equation [41], [42]. The system stability is determined by the zero locations of the characteristic equation, since these zeros are the closed-loop poles of the system.

In addition to the open-loop-gain based analysis with the NSC and the closed-loop-pole based analysis with the characteristic equation, the multi-loop NSC [43] can also be applied to paralleled converter systems. In such a system, by connecting each converter sequentially, which can be seen as closing one more loop each time, a series of open-loop gains can be derived and analysed on Nyquist diagrams for the stability analysis [44]. The benefit of this approach is that it does not require to know the exact number of RHP poles during each time of closing the loops.

From the above perspectives, it is found that the number of RHP poles and zeros in impedance models are critical to the stability analysis. However, this information may be unclear for a "black-box" system. Although the multi-loop NSC can avoid counting the number of open-loop RHP poles, it requires to know the entire network structure to consider the connection sequence of multiple converters for the calculation of open-loop gains, which may not be available for "black-box" systems. This arouses interest to *develop more general stability analysis approach that is readily applicable for "black-box" systems*.

1.2.3. CONTROL DESIGN FOR STABILITY ENHANCEMENT

The impedance-based stability analysis can benefit to the control design of converter systems. When the impedance models of different subsystems at the point of connection can be derived, how they contribute the system stability can be further understood by analysing their impedance profiles on Bode diagrams. Then, the controller impacts on the impedance shaping can be further investigated, and be used as guidelines for control design.

The idea was initially developed in dc distributed systems represented by SISO models. The impedance ratio can be separated as individual impedance models. By comparing their magnitude and phase relationships, one can specify the impedance model of one subsystem to make the system stabilized [40].

Later on, when the impedance-based analysis is applied for ac systems, the passivity-based stability analysis is adopted [19]. If the converter impedance model can be designed as a passive system, which means that the impedance model always has positive real part for all frequencies [45], it will not introduce instability issues when interacting with any passive grid impedances. Although the passivity cannot be achieved in the full frequency range for converter impedances due to the control impacts, the system stability can still be improved by minimizing the non-passive frequency range.

This principle has been widely applied to the control design of grid-following converters, which are controlled as current sources based on the voltage synchronization [5]. The passivity-based current controller design has been studied to enhance the system stability in grid-connected scenarios [46]-[48], by which it is possible to achieve the passivity till half of the sampling frequency. However, the passivity-based impedance design is hardly achievable in the low-frequency range, due to the impacts of outer control loops, such as the phase-locked loop [11] and the dc-link voltage control [49] that are used in grid-following converters. The non-passivity of grid-following converters can be introduced by the negative resistance in the dd or the qq channel of the converter output impedance in the rectifier mode or the inverter mode, respectively [11], [49], since the negative resistance of the diagonal impedance elements provides a sufficient condition for the non-passivity of the

impedance matrix [50]. The instability induced by these low-frequency negative resistances can also be enhanced by reducing the frequency range of the negative resistance [12], [51].

In recent years, the grid-forming control, which regulates the converter as a voltage source based on the power synchronization [52], [53], has become more popular due to their superior stability performance in weak grids [54]-[57]. However, they may also confront instability issues in stiff grids [5], [58]. Although some studies have performed the accurate modelling and stability analysis for grid-forming converters by the state-space analysis [59], [60] or the impedance-based analysis [61], [62], *the control-loop impacts on the impedance shaping of grid-forming converters have not been revealed explicitly, which provides less insight into the control design of grid-forming converters for stability enhancement.*

1.3. OBJECTIVES

Considering the research gaps in the modeling, stability analysis, and control design of grid-interactive converters, this Ph.D. thesis focuses on the following specific objectives.

- *Frequency-domain model development and validation for three-phase converters in unbalanced grid conditions*
- *Impedance-based stability analysis approach that is applicable for "black-box" systems*
- *Control impact investigation and stabilizing solutions to the harmonic stability of grid-forming converters*

1.4. ASSUMPTION AND METHODOLOGY

This Ph.D. thesis deals with the frequency-domain modeling and stability analysis of grid-connected converters, which is based on the following assumptions:

- The converter-based system is assumed to be time periodic in steady state, such that its small-signal stability can be analysed based on a linearized model around the steady state [63].
- It is assumed that the small-signal dynamics of converter systems satisfy the harmonic balance [64], such that a frequency-domain transfer function model can be derived to characterize the converter input-output dynamics. And such a transfer function model can be measured by frequency scan.
- The open-loop gain (i.e., the impedance ratio) of the interconnected converter system can be defined as proper, such that the NSC can be applied for stability analysis [36].

Based on the above assumptions, the following methods will be adopted for the modeling, stability analysis, and validations:

- For the model derivation, the *linearization based on Taylor series* [65] will be applied in the time domain to derive the small-signal model, while the *frequency-domain analysis approaches* will be used to derive the frequency-domain transfer function models for both LTP [66] or LTI systems. The *complex variables and complex transfer functions* [22] will be utilized to represent the models in the complex $\alpha\beta$ or dq frame.
- For the model validation, the *frequency-scan technique* [15]-[17], [67] will be used for the impedance measurement. The obtained frequency-scanned impedance of a "black-box" converter system will be compared with the analytical model for validation.
- For stability analysis, the *Nyquist stability criterion* and *closed-loop pole analysis* will be conducted on the obtained frequency-domain models [36].
- For stability validation, *electromagnetic transient (EMT) simulations and experiments* on three-phase converters will be conducted. The critical stability conditions in the time domain will be compared with those in the frequency-domain stability analysis for validation.

1.5. THESIS OUTLINE AND CONTRIBUTIONS

This Ph.D. thesis is composed of five chapters. The main chapters are related to five publications [J1]-[J5].

Chapter 1 is the Introduction.

Chapter 2 develops unified frequency-domain modeling approaches for grid-interactive converters, which is divided into two sections.

- Section 2.1 [J1]: *stationary-frame impedance modeling and measurement*
  The stationary-frame impedance modeling for grid-interactive converters in three-phase balanced grids is established first based on a direct linearization in the $\alpha\beta$ frame. The frequency-coupling and phase-dependent dynamics are revealed by the analytical model, based on which a frequency-scan approach to the impedance measurement is proposed.
- Section 2.2 [J2]: *impedance modeling of converters in unbalanced grids*
  The derived stationary-frame impedance model of three-phase converters in Section 2.1 is generalized to unbalanced grid conditions considering more frequency coupling dynamics. The derived model is further validated by the frequency scan approach proposed in Section 2.1.

Chapter 3 focuses on the impedance-based stability analysis approaches, which is divide into two sections.

- Section 3.1 [J3]: *stability analysis with SISO impedance models*
  For interconnected system with SISO impedance models, the stability can be analyzed by applying the NSC to the impedance ratio. A general impedance-based stability analysis approach considering the existence of RHP poles is proposed, which enables to identify the number of open-loop RHP poles directly from individual impedance Bode diagrams and to implement the impedance specification.
- Section 3.2 [J2]: *stability analysis with MIMO impedance models*
  Two different ways to analyze the stability with MIMO impedance models are introduced. One is based on open-loop gain analysis with the generalized NSC, and the other is based on the closed-loop pole analysis with the characteristic equation. They can be both analyzed with equivalent SISO models. A case study of grid-interactive converter in unbalanced grid conditions is conducted to validate the two approaches.

Chapter 4 further applies the developed analysis approaches to the grid-forming converters for control design and stability enhancement, which is divided into two sections.

- Section 4.1 [J4]: *passivity-based analysis for voltage control of grid-forming converters*
  The high-frequency harmonic instability issues caused by the voltage control of grid-forming converters in grid-connected applications are studied first. The negative resistance caused by different voltage control schemes is derived, and a passivity-based controller co-design approach is proposed, which solves the high-frequency harmonic instability issues till half of the sampling frequency.
- Section 4.2 [J5]: *control-loop impact analysis of grid-forming converters*
  Considering the outer-loop control dynamics, the sideband oscillations of grid-forming converters in stiff grids are studied with the impedance analysis. The instability mechanism is clarified based on the small-gain theorem. An impedance decomposition method is further developed to analyze the control-loop impacts, which helps explain how each control loop affects the sideband oscillations.

Chapter 5 finally concludes the thesis and provides the prospects.

The unique contributions of this Ph.D. thesis can be summarized in the following aspects:

- A frequency scan approach that measures the converter frequency-domain models in the stationary reference frame has been proposed, which can be used for modeling of “black-box” systems.

- A unified multi-frequency stationary-frame impedance model for three-phase converters has been proposed, which works for both balanced and unbalanced grid conditions and can be used for system stability analysis.
- A general impedance-based stability analysis approach that is applicable for "black-box" systems has been proposed, which allows for the impedance specification even with the existence of open-loop RHP poles.
- A control co-design method for the voltage loop of grid-forming converters is proposed, which realizes the impedance passivity till half of the sampling frequency and improve the stability in grid-connected applications.
- An impedance decomposition approach to characterizing different control-loop impacts has been developed for grid-forming converters, based on which the control-loop impacts on the sideband oscillations can be revealed from the small-gain perspective.

1.6. RELATED PUBLICATIONS

The publications related to this Ph.D. thesis are listed as follows:

[J1] **Yicheng Liao** and Xiongfei Wang, "Stationary-Frame Complex-Valued Frequency-Domain Modeling of Three-Phase Power Converters," ***IEEE Journal of Emerging and Selected Topics in Power Electron*ics**, vol. 8, no. 2, pp. 1922-1933, Jun. 2020.

[J2] **Yicheng Liao**, Xiongfei Wang, Xiaolong Yue, and Lennart Harnefors, "Complex-Valued Multi-Frequency Admittance Model of Three-Phase VSCs in Unbalanced Grids," ***IEEE Journal of Emerging and Selected Topics in Power Electron*ics**, vol. 8, no. 2, pp. 1934-1946, Jun. 2020.

[J3] **Yicheng Liao** and Xiongfei Wang, "Impedance-Based Stability Analysis for Interconnected Converter Systems with Open-Loop RHP Poles," ***IEEE Transactions on Power Electron*ics**, vol. 35, no. 4, pp. 4388-4397, Apr. 2020.

[J4] **Yicheng Liao**, Xiongfei Wang, and Frede Blaabjerg, "Passivity-Based Analysis and Design of Linear Voltage Controllers For Voltage-Source Converters," ***IEEE Open Journal of the Industrial Electronics Society***, vol. 1, pp. 114-126, 2020.

[J5] **Yicheng Liao** and Xiongfei Wang, "Impedance Decomposition for Design-Oriented Analysis of Grid-Forming Voltage-Source Converters," ***IEEE TechRxiv***, Aug. 2020, DOI: 10.36227/techrxiv.12855167.

CHAPTER 2. FREQUENCY-DOMAIN MODELING METHODS OF THREE-PHASE CONVERTERS

"A physical law must possess mathematical beauty."

— P. A. M. Dirac

This chapter develops the frequency-domain approaches to three-phase grid-interactive converters. First, the stationary-frame impedance modeling and validation of converters in balanced grids are studied in Section 2.1. Then, the model is generalized in unbalanced grids in Section 2.2.

2.1. STATIONARY-FRAME IMPEDANCE MODELING AND MEASUREMENT

The stationary-frame impedance modeling and measurement approaches to grid-interactive converters are developed in this section, based on the content in the Publication [J1].

2.1.1. BACKGROUND

The impedance modeling of grid-interactive converters in balanced grid conditions has been derived in the real *dq* frame [12], the complex *dq* frame [24], and the *αβ* frame [27]. Figure 2-1 shows the general modeling principles of these methods.

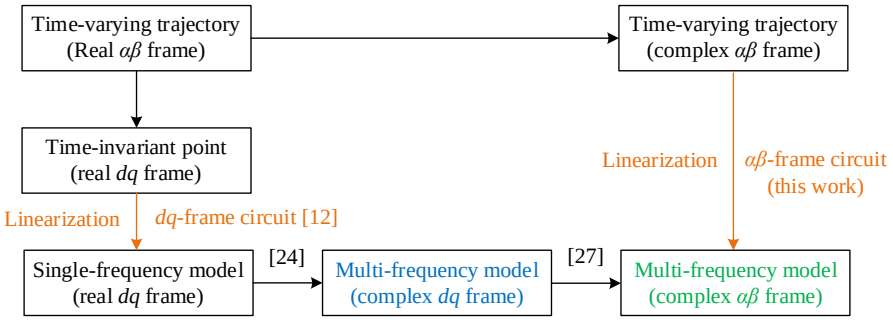

Figure 2-1 Modeling principles of existing works and this work. Source: [J1].

The real *dq*-frame model linearizes the converter system in dq frame around the time-invariant operating points [12], which leads to an LTI system. Therefore, the resulted model is a single-frequency model, which, however, cannot reveal the frequency

coupling dynamics. To capture the frequency-coupling dynamics, the real *dq*-frame model can be derived in the complex *dq* frame by a real-to-complex coordinate transformation [24], and further derived in the complex $\alpha\beta$ frame through an inverse Park transformation [27]. Compared with *dq* frame models, the $\alpha\beta$ frame model directly reveals the frequency-coupling phenomena observed in the phase domain. However, the model derived in [27] is merely based on mathematical derivations from the *dq* frame models. Although the frequency-coupling dynamics are revealed, the phase-dependent effects are not considered, which brings challenges to the impedance measurement in the stationary frame.

A frequency-scan method to measuring converter impedance model in the stationary frame has been recently studied in [67]. Although the phase dependence brought by the frequency couplings has been considered in the measurement, the off-diagonal elements cannot be measured directly. Furthermore, the method also relies on the use of test impedances, which makes the implementation more difficult.

This challenge is thus studied in this work. By a direct linearization in the $\alpha\beta$ frame, the converter power stage is modeled by an equivalent three-port model. Such a model reveals the frequency-coupling and phase-dependent dynamics in the converter system. The three-port model can also be integrated with converter controls to derive any closed-loop transfer functions. Based on the analytical modeling, a stationary-frame impedance measurement approach is also proposed, where the importance to consider the phase dependence in the impedance measurement is highlighted. Compared with the method in [67], the proposed impedance measurement approach directly measures all the elements in the impedance matrix, which does not need the aid of any test impedances.

2.1.2. IMPEDANCE MODELING BASED ON THREE-PORT MODEL

The impedance modeling of a grid-following converter is studied in this work. Figure 2-2 shows the converter control diagram. The phase-locked loop (PLL), the dc-link voltage control (DVC) and the current control (CC) are considered.

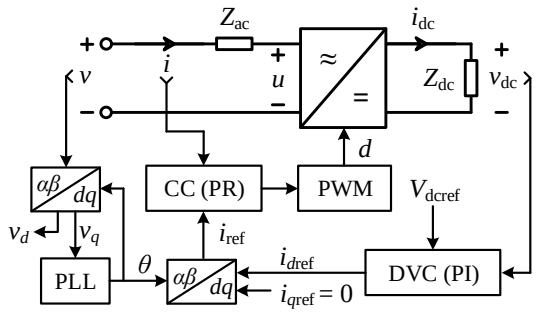

Figure 2-2 Studied three-phase grid-following converter in single-line representation. Source: [J1].

Using the complex space vectors defined in the $\alpha\beta$ frame, i.e., $\mathbf{v}=v_\alpha+jv_\beta$ and $\mathbf{v}^*=v_\alpha-jv_\beta$, the linearization can be directly done in the stationary frame, yielding an equivalent circuit model of the converter power stage, as given in Figure 2-3. The explicit linearization derivation can be found in [J1]. It can be seen that the ac-side circuit corresponds to two ports, whose signals are defined as $\left[\hat{\mathbf{v}}, e^{j2\theta_1}\hat{\mathbf{v}}^*\right]^{\mathrm{T}}$ and similar to other ac variables. In contrast, the dc side circuit corresponds to a single port, whose signal can be defined as $e^{j\theta_1}\hat{v}_{\mathrm{dc}}$ and similar to other dc variables. Here, in the exponential functions of $e^{j2\theta_1}$ and $e^{j\theta_1}$, $\theta_1 \triangleq \omega_1 t+\varphi_1$ is the phase of the steady-state voltage trajectory at the point of connection. These exponential functions are intentionally combined with signals, to ensure that the derived frequency-domain models are still LTI. Consequently, the frequency couplings and phase dependence of the converter system can be clarified, since these signals are mapped into the frequency domain as

$$\begin{bmatrix}\mathbf{v}\\ e^{j2\theta_1}\mathbf{v}^*\end{bmatrix}\leftrightarrow\begin{bmatrix}\mathbf{V}(s)\\ e^{j2\varphi_1}\mathbf{V}^*(s-j2\omega_1)\end{bmatrix}=\begin{bmatrix}V_\alpha(s)+jV_\beta(s)\\ e^{j2\varphi_1}\left(V_\alpha(s-j2\omega_1)-jV_\beta(s-j2\omega_1)\right)\end{bmatrix} \tag{2-1}$$

$$e^{j\theta_1}v_{\mathrm{dc}}\leftrightarrow e^{j\varphi_1}V_{\mathrm{dc}}(s-j\omega_1) \tag{2-2}$$

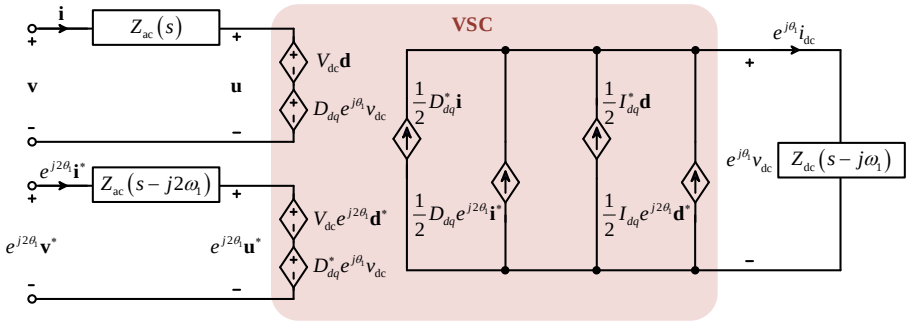

Figure 2-3 Linearized three-port model of converter power stage in stationary frame. Source: [J1].

Based on the three-port model, the open-loop transfer function models of the converter power stage can be derived as Figure 2-4, where the inputs are ac voltage and duty cycle vectors, and the outputs are dc voltage and ac current. The corresponding transfer function matrices can be derived as

$$\left[\mathbf{Z}_{\text{ol}}\right]_{2\times2}=\mathbf{Z}_{\text{ac}}+\frac{1}{2}Z_{\text{dc}}\left(s-j\omega_1\right)\begin{bmatrix}D_{dq}D_{dq}^* & D_{dq}^2\\ D_{dq}^{*2} & D_{dq}D_{dq}^*\end{bmatrix} \tag{2-3}$$

$$\left[\mathbf{G}_{\text{di}}\right]_{2\times2}=-\mathbf{Z}_{\text{ol}}^{-1}\left(V_{\text{dc}}\begin{bmatrix}1 & \\ & 1\end{bmatrix}+\frac{Z_{\text{dc}}\left(s-j\omega_1\right)}{2}\begin{bmatrix}D_{dq}I_{dq}^* & D_{dq}I_{dq}\\ D_{dq}^*I_{dq}^* & D_{dq}^*I_{dq}\end{bmatrix}\right) \tag{2-4}$$

$$\left[\mathbf{G}_{\text{vv}}\right]_{1\times2}=\frac{\frac{Z_{\text{dc}}\left(s-j\omega_1\right)}{2}\begin{bmatrix}D_{dq}^* & D_{dq}\end{bmatrix}\mathbf{Z}_{\text{ac}}^{-1}}{1+\frac{Z_{\text{dc}}\left(s-j\omega_1\right)}{2}\begin{bmatrix}D_{dq}^* & D_{dq}\end{bmatrix}\mathbf{Z}_{\text{ac}}^{-1}\begin{bmatrix}D_{dq}\\ D_{dq}^*\end{bmatrix}} \tag{2-5}$$

$$\left[\mathbf{G}_{\text{dv}}\right]_{1\times2}=\frac{\frac{Z_{\text{dc}}\left(s-j\omega_1\right)}{2}\left(\begin{bmatrix}I_{dq}^* & I_{dq}\end{bmatrix}-V_{\text{dc}}\begin{bmatrix}D_{dq}^* & D_{dq}\end{bmatrix}\mathbf{Z}_{\text{ac}}^{-1}\right)}{1+\frac{Z_{\text{dc}}\left(s-j\omega_1\right)}{2}\begin{bmatrix}D_{dq}^* & D_{dq}\end{bmatrix}\mathbf{Z}_{\text{ac}}^{-1}\begin{bmatrix}D_{dq}\\ D_{dq}^*\end{bmatrix}} \tag{2-6}$$

In the above equations, V_{dc}, D_{dq}, I_{dq} are steady-state values. $Z_{\text{dc}}(s)$ is the dc-side impedance transfer function, while $Z_{\text{ac}}(s)$ is the ac-side impedance transfer function, giving the matrix $\mathbf{Z}_{\text{ac}}$ as

$$\left[\mathbf{Z}_{\text{ac}}\right]_{2\times2}=\begin{bmatrix}Z_{\text{ac}}\left(s\right) & \\ & Z_{\text{ac}}\left(s-j2\omega_1\right)\end{bmatrix} \tag{2-7}$$

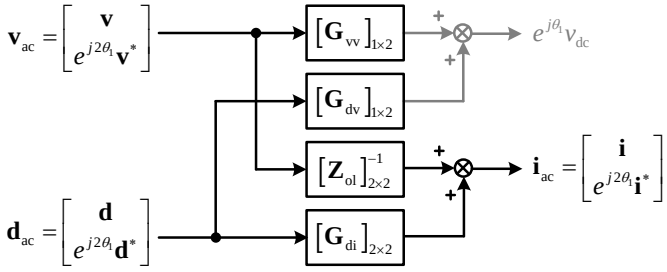

Figure 2-4 Open-loop model of the converter power stage. Source: [J1].

Then, considering the linearized modeling of different control blocks, the closed-loop model the converter can be derived as Figure 2-5. $\mathbf{Y}_{\mathrm{PLL}}$ characterizes the dynamic of the PLL and $\mathbf{Y}_{\mathrm{DVC}}$ characterizes the dynamic of the DVC. Since PLL provides the voltage phase θ and the DVC provides the d-axis current reference $i_{d\mathrm{ref}}$, they are combined in the current reference generation through the inverse Park transformation. By linearizing this process, the expressions of $\mathbf{Y}_{\mathrm{PLL}}$ and $\mathbf{Y}_{\mathrm{DVC}}$ can be derived as

$$\left[\mathbf{Y}_{\mathrm{PLL}}\right]_{2\times2}=\begin{bmatrix}\frac{I_{dq\mathrm{ref}}}{2}G_{\mathrm{PLL}}\left(s-j\omega_1\right) & -\frac{I_{dq\mathrm{ref}}}{2}G_{\mathrm{PLL}}\left(s-j\omega_1\right)\\ -\frac{I^*_{dq\mathrm{ref}}}{2}G_{\mathrm{PLL}}\left(s-j\omega_1\right) & \frac{I^*_{dq\mathrm{ref}}}{2}G_{\mathrm{PLL}}\left(s-j\omega_1\right)\end{bmatrix} \tag{2-8}$$

$$\left[\mathbf{Y}_{\mathrm{DVC}}\right]_{2\times1}=\begin{bmatrix}G_{\mathrm{DVC}}\left(s-j\omega_1\right)\\ G_{\mathrm{DVC}}\left(s-j\omega_1\right)\end{bmatrix} \tag{2-9}$$

where $G_{\mathrm{PLL}}(s)$ denotes the closed-loop transfer function of the PLL [12] and $G_{\mathrm{DVC}}(s)$ is the transfer function of the dc-link voltage controller.

For the current controller and the time delay, they are represented by $\mathbf{G}_{\mathrm{i}}$ and $\mathbf{G}_{\mathrm{d}}$ in Figure 2-5. Since these transfer functions are LTI in the $\alpha\beta$ frame, they can be derived only considering a frequency shift caused by $e^{j2\theta_1}$ in the second diagonal element as

$$\left[\mathbf{G}_{\mathrm{i}}\right]_{2\times2}=\begin{bmatrix}G_{\mathrm{i}}\left(s\right) & \\ & G_{\mathrm{i}}\left(s-j2\omega_1\right)\end{bmatrix} \tag{2-10}$$

$$\left[\mathbf{G}_{\mathrm{d}}\right]_{2\times2}=\begin{bmatrix}G_{\mathrm{d}}\left(s\right) & \\ & G_{\mathrm{d}}\left(s-j2\omega_1\right)\end{bmatrix} \tag{2-11}$$

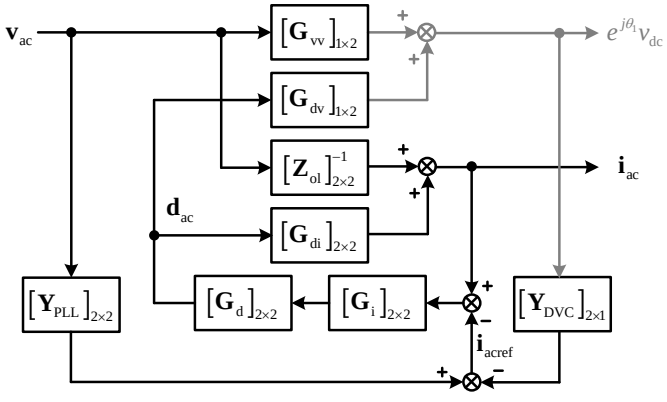

Figure 2-5 Closed-loop model of the converter. Source: [J1].

Considering the model in Figure 2-5, the closed-loop output admittance, which is the transfer function matrix from $\mathbf{v}_{ac}$ to $\mathbf{i}_{ac}$, can be derived as

$$\begin{aligned}\left[\mathbf{Y}_{accl}\right]_{2\times2} = \frac{\mathbf{i}_{ac}}{\mathbf{v}_{ac}} = &\left[\mathbf{I}-\mathbf{G}_{di}\left(\mathbf{I}-\mathbf{G}_{d}\mathbf{G}_{i}\mathbf{Y}_{DVC}\mathbf{G}_{dv}\right)^{-1}\mathbf{G}_{d}\mathbf{G}_{i}\right]^{-1} \\ &\cdot\left[\mathbf{Z}_{ol}^{-1}-\mathbf{G}_{di}\left(\mathbf{I}-\mathbf{G}_{d}\mathbf{G}_{i}\mathbf{Y}_{DVC}\mathbf{G}_{dv}\right)^{-1}\mathbf{G}_{d}\mathbf{G}_{i}\left(\mathbf{Y}_{PLL}-\mathbf{Y}_{DVC}\mathbf{G}_{vv}\right)\right]\end{aligned} \tag{2-12}$$

It is noted that the model in Figure 2-5 is the entire frequency-domain model. In addition to the ac-side impedance, any other closed-loop transfer functions can be derived.

2.1.3. IMPEDANCE MEASUREMENT APPROACH

The impedance measurement approach based on frequency scan can be developed based on the three-port model, considering the frequency-coupling and phase-dependent dynamics. The flowchart of the impedance measurement approach is given in Figure 2-6, including the perturbation injection, response analysis and the impedance calculation. It is noted that the principle also applies to obtain frequency responses of any other transfer function matrices.

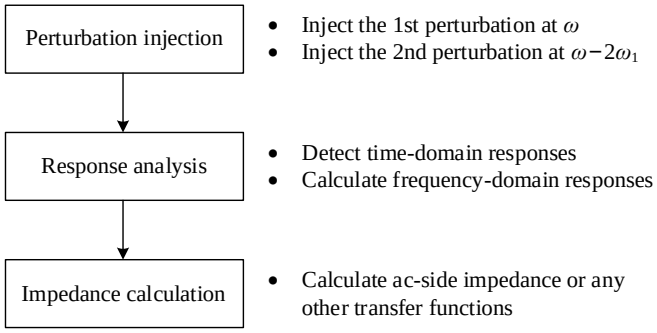

Figure 2-6 Flowchart of the impedance measurement approach in the stationary frame.

Perturbation Injection: Since the impedance model is a two-by-two matrix at the ac side, it is necessary to inject two perturbations to get the full dynamic responses of the entire system. The two perturbations are independent. The first is generated at ω, based on the definition of the first vector, i.e, $\mathbf{v}=v_\alpha+jv_\beta$, indicating that the initial phase of the β-axis sinusoidal signal is lagging 90° of the α-axis sinusoidal signal. The second perturbation can be designed based on the second vector, i.e., $e^{j2\theta_1}\mathbf{v}^*=e^{j2\theta_1}\left(v_\alpha-jv_\beta\right)$. The initial phase of the β-axis sinusoidal signal is leading 90° of the α-axis sinusoidal signal, yet the frequency is at $\omega-2\omega_1$.

Response Analysis: Under two perturbations, the time-domain responses of the ac-side voltage ($v_{\alpha k}$, $v_{\beta k}$) and the current ($i_{\alpha k}$, $i_{\beta k}$) can be detected, where k = 1, 2, indicating the measurement sequence. Then, the frequency responses can be analyzed according to (2-1) and (2-2), yielding

$$\begin{bmatrix}\mathbf{V}_k(\omega)\\ e^{j2\varphi_{1k}}\mathbf{V}_k^*(\omega-2\omega_1)\end{bmatrix}=\begin{bmatrix}\mathcal{F}\{v_{\alpha k}(\omega)\}+j\mathcal{F}\{v_{\beta k}(\omega)\}\\ e^{j2\varphi_{1k}}\left(\mathcal{F}\{v_{\alpha k}(\omega-2\omega_1)\}-j\mathcal{F}\{v_{\beta k}(\omega-2\omega_1)\}\right)\end{bmatrix} \tag{2-13}$$

$$\begin{bmatrix}\mathbf{I}_k(\omega)\\ e^{j2\varphi_{1k}}\mathbf{I}_k^*(\omega-2\omega_1)\end{bmatrix}=\begin{bmatrix}\mathcal{F}\{i_{\alpha k}(\omega)\}+j\mathcal{F}\{i_{\beta k}(\omega)\}\\ e^{j2\varphi_{1k}}\left(\mathcal{F}\{i_{\alpha k}(\omega-2\omega_1)\}-j\mathcal{F}\{i_{\beta k}(\omega-2\omega_1)\}\right)\end{bmatrix} \tag{2-14}$$

Impedance measurement: Then the ac-side impedance matrix can be calculated by

$$\begin{bmatrix}\mathbf{Y}_{ac11}(\omega) & \mathbf{Y}_{ac12}(\omega)\\ \mathbf{Y}_{ac21}(\omega) & \mathbf{Y}_{ac22}(\omega)\end{bmatrix}=\begin{bmatrix}\mathbf{I}_1(\omega) & \mathbf{I}_2(\omega)\\ e^{j2\varphi_{11}}\mathbf{I}_1^*(\omega-2\omega_1) & e^{j2\varphi_{12}}\mathbf{I}_2^*(\omega-2\omega_1)\end{bmatrix}\cdot\begin{bmatrix}\mathbf{V}_1(\omega) & \mathbf{V}_2(\omega)\\ e^{j2\varphi_{11}}\mathbf{V}_1^*(\omega-2\omega_1) & e^{j2\varphi_{12}}\mathbf{V}_2^*(\omega-2\omega_1)\end{bmatrix}^{-1} \tag{2-15}$$

This frequency-scan approach can also be applied to measure any other transfer functions.

2.1.4. EXPERIMENTAL RESULTS

The cross validation of the impedance modeling and measurement approaches is conducted by experiments on a grid-connected converter. Figure 2-7 shows the experimental setup. The three-phase grid voltage is emulated by a grid simulator (Chroma 61845). Three-phase LC filters are used to emulate the grid impedances. At the point of connection (PoC), an L-filtered voltage-source converter (VSC1) with grid-following control is connected. Its ac-side impedance is measured by injecting current perturbations using the VSC2. The circuit and control parameters can be found in [J1].

The impedance of VSC1 is calculated by measuring the responses *v* and *i* at the PoC. The frequency is scanned within (0, 200)Hz, since in this frequency range the frequency couplings are most significant. Figure 2-8 shows the experimental result in contrast to the analytical model. The solid lines represent the analytical models obtained by (2-12), while the crosses represent the frequency-scanned results obtained by (2-15). Two cases are studied. Case A is for the converter working in the inverter mode, and Case B is for the rectifier mode. It can be seen that under both conditions, the experimental results show good agreements with the analytical models. Especially, for the off-diagonal elements in the impedance matrix, only when the phase dependence is considered, can these elements be accurately measured.

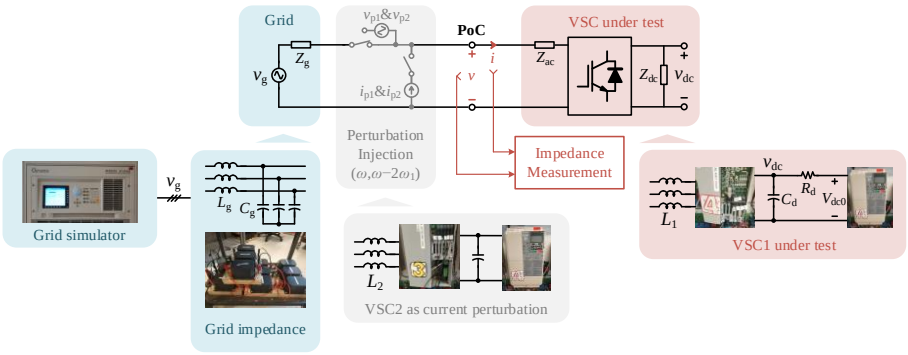

Figure 2-7 Experimental setup for impedance measurement. Source: [J1].

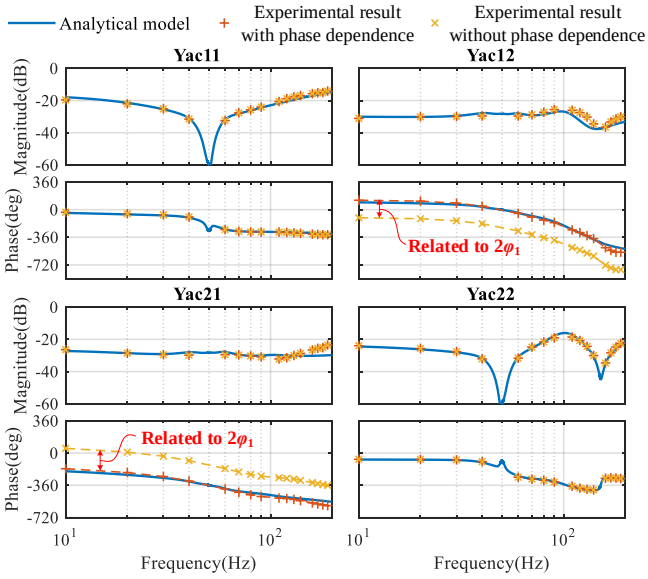

(a)

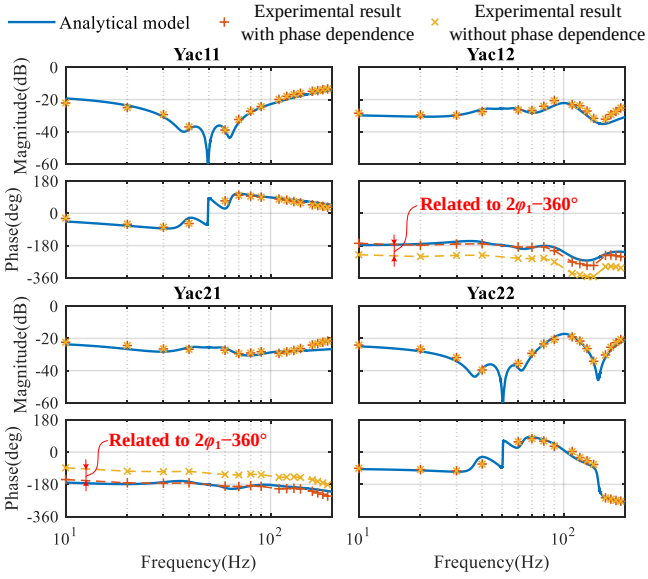

(b)

Figure 2-8 Experimental results for impedance measurement. (a) Case A – inverter mode; (b) Case B – rectifier mode. Source: [J1].

2.1.5. SUMMARY

The linearized three-port circuit model is proposed to modeling the three-phase converter power stage in the stationary frame, which can be used to derive the frequency-domain transfer functions of converters in balanced grid conditions. It is revealed that the frequency-coupling and phase-dependent dynamics are characterized in both ac- and dc-side signals, which need to be considered for the impedance measurement. A frequency-scan approach considering the frequency-coupling and phase-dependent dynamics is thus developed for the impedance measurement of converters. Experimental results verifies that the model can be well applied for "black-box" systems, since the impedances can be accurately measured by frequency scan without knowing the converter internal parameters.

2.2. IMPEDANCE MODELING IN UNBALANCED GRIDS

The stationary-frame impedance modeling approach to grid-interactive converters in unbalanced grids is developed in this section, based on the content in the Publication [J2].

2.2.1. BACKGROUND

The well-developed dq-frame or $\alpha\beta$-frame impedance models of grid-interactive converters are all two-by-two matrices in the frequency domain, which only work for the balanced grid conditions. Under unbalanced grid conditions, no matter the converter is modeled in dq frame or $\alpha\beta$ frame, the voltage will always feature time periodicity in steady states, which requires to model the system considering multiple harmonics.

The dynamic phasor modeling based on generalized averaging can be utilized for three-phase unbalanced systems [68]-[70], yet the model is mainly derived with the state-space form in the time domain. Alternatively, the HSS modeling for LTP systems [66] can be applied, by which the harmonic transfer functions (HTFs) model the system dynamics in the frequency domain [29]-[31]. This method has been recently used to model the impedance model of converters in unbalanced grid conditions [33]. However, the model derived in [33] relies on the couplings from unbalanced grid impedances, thus the derived model is not the actual converter impedance model at the point of connection. In addition, it overlooks the complex frequency-coupling dynamics caused by the PLL [71].

Considering the drawbacks of the model in [33], this work intends to develop the impedance model for grid-interactive converters in unbalanced grids. The HSS modeling is adopted to characterize the harmonic impacts of the unbalanced voltage trajectory. The model is also derived in the stationary frame using complex vectors, thus it extends the conventional HSS modeling theory in the complex domain. The

complex frequency dynamics impacted by the PLL structures are studied comprehensively, and its implication to model order truncation is also pointed out. Differing from [33], the derived converter impedance model merely relies on the steady-state trajectory of the voltage at the point of connection, which can be validated by impedance measurement.

2.2.2. PLL MODELING

A grid-following converter is studied in this case. Since the PLL is the mostly essential control block for the converter synchronization in the unbalanced grids, this work considers the PLL as the only outer loop. The converters with other outer control loops can be modeled using the same approach. The control diagram of the studied system is given in Figure 2-9. Considering the unbalanced grid conditions, the conventional synchronous-reference-frame PLL (SRF-PLL) and the notch-filtered PLL (Notch-SRF-PLL) are both studied, whose control diagrams are shown in Figure 2-10.

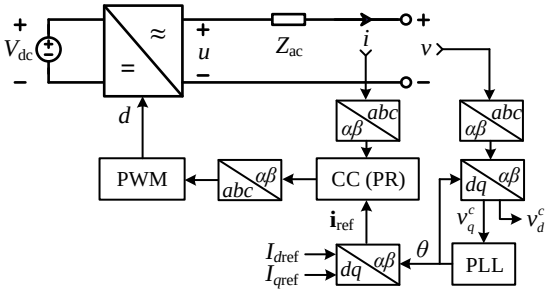

Figure 2-9 Control scheme of the grid-following converter in unbalanced grids. Source: [J2].

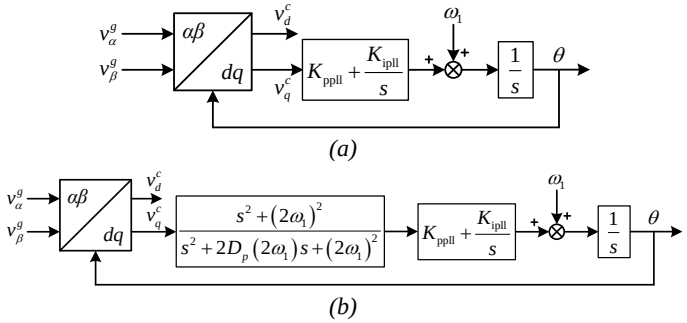

Figure 2-10 Control diagrams of PLLs. (a) SRF-PLL; (b) Notch-SRF-PLL. Source: [J2].

For the SRF-PLL, the locked phase θ is not equal to the positive-sequence voltage phase θ^+. Therefore, a steady-state phase error exists between the two phases, i.e.,

$\theta=\theta^{+}+\Delta\theta$ [71]. Theoretically, $\Delta\theta$ is non-negligible with the unbalanced grid voltage input, such that three time-periodic trajectories will be involved in the PLL modeling, i.e., $\sin\Delta\theta(t)$, $\cos\Delta\theta(t)$, and $V_d^c(t)$, yielding the small-signal model given in Figure 2-11. Then, the HTF of the SRF-PLL is derived as

$$\mathbf{\Theta}(s)=\underbrace{\left(\mathcal{I}+\mathcal{G}_{\text{PI-I}}(s)\mathcal{V}_d^c\right)^{-1}\mathcal{G}_{\text{PI-I}}(s)}_{\left[\mathcal{G}_{\text{PLL}}(s)\right]_{n\times n}}\underbrace{\left(\mathcal{T}_{\cos\Delta\theta}\mathbf{V}_q^g(s)-\mathcal{T}_{\sin\Delta\theta}\mathbf{V}_d^g(s)\right)}_{\mathbf{V}_q'^g(s)} \tag{2-16}$$

In contrast, for the Notch-SRF-PLL, the locked phase θ is exactly the same as the positive-sequence voltage phase θ^{+} in steady state. Consequently, $\sin\Delta\theta(t)=0$, $\cos\Delta\theta(t)=1$, and $V_d^c(t)$ is the only time-periodic trajectory in the small-signal model. Figure 2-12 displays the small-signal model of the Notch-SRF-PLL with unbalanced voltages. And its HTF model can be derived as

$$\mathbf{\Theta}(s)=\underbrace{\left(\mathcal{I}+\mathcal{G}_{\text{Notch-PI-I}}(s)\mathcal{V}_d^c\right)^{-1}\mathcal{G}_{\text{Notch-PI-I}}(s)}_{\left[\mathcal{G}_{\text{PLL}}(s)\right]_{3\times 3}}\mathbf{V}_q^g(s) \tag{2-17}$$

Comparing the two PLL models, it can be found that SRF-PLL features more complicated frequency-coupling dynamics, since it has three steady-state time-periodic coefficients, and they are all composed of infinite harmonics of $2k\omega_1$, theoretically. As for the Notch-SRF-PLL, since $\sin\Delta\theta(t)=0$ and $\cos\Delta\theta(t)=1$ hold in steady state, it largely simplify the harmonic spectrum of $V_d^c(t)$. $V_d^c(t)$ only have finite order of harmonics at 0 rad/s and $\pm2\omega_1$, which contributes to the HTF model truncation.

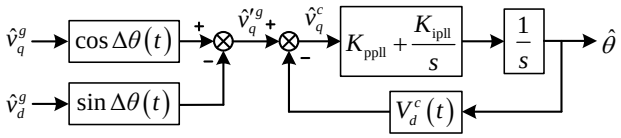

Figure 2-11 Small-signal model of SRF-PLL with unbalanced voltages. Source: [J2].

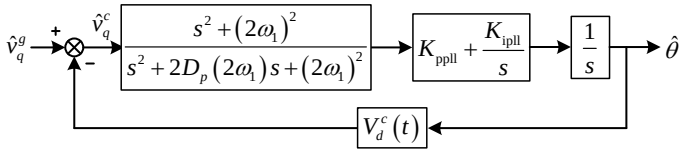

Figure 2-12 Small-signal model of Notch-SRF-PLL with unbalanced voltages. Source: [J2].

It is noted that the derived HTF models in (2-16) and (2-17) are both represented in the real *dq* frame, which can be further transformed into the complex *dq* frame in order to derive the model in the stationary frame.

2.2.3. CONVERTER MODELING

The PLL dynamic can be incorporated into the current control through the current reference generation. Figure 2-13 provides the derivation process of the PLL dynamics in the complex $\alpha\beta$ frame. $\mathcal{G}_{\text{PLL}}(s)$ is the closed-loop HTF of the PLL, which are derived previously in (2-16) or (2-17). If the input voltage is represented by the two complex vectors, i.e., $\left[\hat{\mathbf{v}}^{g}, e^{j2\theta^{+}}\hat{\mathbf{v}}^{g*}\right]^{\mathrm{T}}$, then the PLL dynamics can be represented by the transformations shown in the blue block diagram. Linearizing the current reference generation yields the transformations in the red block diagram. To generate the same output signal form of the current reference as the voltage input, the conjugate operation is applied, yielding the second path represented by the dashed arrows. Then the diagram in Figure 2-13(a) can be simplified as the model in Figure 2-13(b), such that the transfer function matrix from the input voltage vector to the current reference vector can be derived as $\mathbf{Y}_{\text{PLL}}(s)$, i.e.,

$$\mathbf{Y}_{\text{PLL}}(s)=\frac{1}{2}\begin{bmatrix} I_{dq\text{ref}}\mathcal{T}_{\Delta\theta}\mathcal{G}_{\text{PLL}}(s-j\omega_1)\mathcal{T}_{\Delta\theta}^{*} & -I_{dq\text{ref}}\mathcal{T}_{\Delta\theta}\mathcal{G}_{\text{PLL}}(s-j\omega_1)\mathcal{T}_{\Delta\theta} \\ -I_{dq\text{ref}}^{*}\mathcal{T}_{\Delta\theta}^{*}\mathcal{G}_{\text{PLL}}(s-j\omega_1)\mathcal{T}_{\Delta\theta}^{*} & I_{dq\text{ref}}^{*}\mathcal{T}_{\Delta\theta}^{*}\mathcal{G}_{\text{PLL}}(s-j\omega_1)\mathcal{T}_{\Delta\theta} \end{bmatrix} \quad (2\text{-}18)$$

where $\mathcal{T}_{\Delta\theta}$ is the HTF of $e^{j\Delta\theta}$.

It is noted that the input represented by two complex vectors is a 2-dimensional (2-D) vector in time domain, corresponding to a 2*n*-D vector in the frequency domain, where $n=2k+1$ and k is the truncated order of the PLL HTF model. The frequency response of the input voltage vector can be represented by

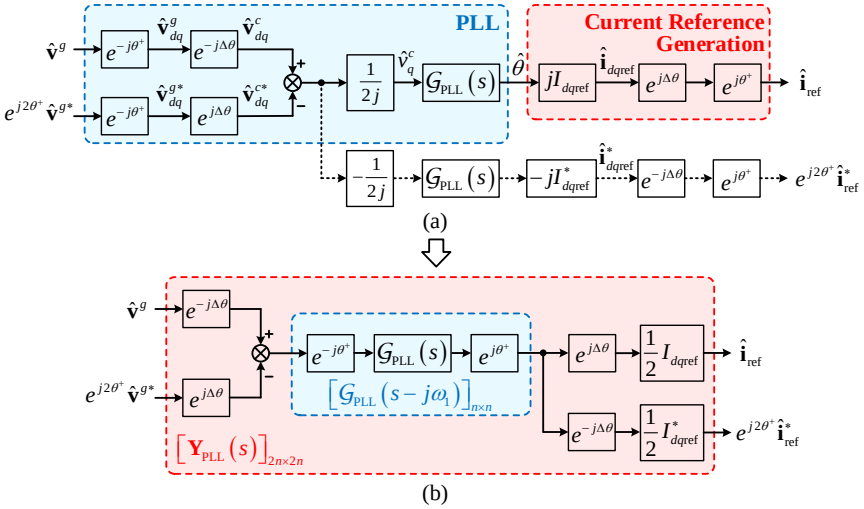

Figure 2-13 Derivation of the PLL dynamics in the stationary frame. (a) Small-signal diagrams of the PLL and the current reference generation; (b) Derivation of $\boldsymbol{Y}_{PLL}(s)$. Source: [J2].

$$\begin{bmatrix} \hat{\mathbf{v}}^{g} \\ e^{j2\theta^{+}}\hat{\mathbf{v}}^{g*} \end{bmatrix} \leftrightarrow \begin{bmatrix} \vdots \\ \mathbf{V}^{g}(s-j2\omega_1) \\ \mathbf{V}^{g}(s) \\ \mathbf{V}^{g}(s+j2\omega_1) \\ \vdots \\ \vdots \\ e^{j2\varphi^{+}}\mathbf{V}^{g*}\left((s-j2\omega_1)-j2\omega_1\right) \\ e^{j2\varphi^{+}}\mathbf{V}^{g*}(s-j2\omega_1) \\ e^{j2\varphi^{+}}\mathbf{V}^{g*}\left((s+j2\omega_1)-j2\omega_1\right) \\ \vdots \end{bmatrix} = \begin{bmatrix} \vdots \\ \mathbf{V}^{g}(s-j2\omega_1) \\ \mathbf{V}^{g}(s) \\ \mathbf{V}^{g}(s+j2\omega_1) \\ \vdots \\ \vdots \\ e^{j2\varphi^{+}}\mathbf{V}^{g*}(s-j4\omega_1) \\ e^{j2\varphi^{+}}\mathbf{V}^{g*}(s-j2\omega_1) \\ e^{j2\varphi^{+}}\mathbf{V}^{g*}(s) \\ \vdots \end{bmatrix} \tag{2-19}$$

The frequency couplings between $\hat{\mathbf{v}}^{g}$ and $e^{j2\theta^{+}}\hat{\mathbf{v}}^{g*}$ are introduced by the asymmetrical *dq* control dynamics, which are the same as observed in the balanced cases. As for the frequency couplings introduced in each complex vector, they are resulted from the time periodicity caused by the unbalanced voltage trajectory. Therefore, this model generalizes the stationary-frame impedance model derived in the Section 2.1 to the unbalanced grid conditions.

Considering these frequency coupling dynamics, the current control, time delay, and the converter plant models can all be represented with HTFs. Since they are all LTI systems, the HTFs can be denoted by frequency-shifted LTI transfer functions as diagonal elements, i.e.,

$$\mathbf{G}(s) = diag\begin{Bmatrix} \cdots, G(s-j2\omega_1), G(s), G(s+j2\omega_1), \cdots, \\ \cdots, G(s-j4\omega_1), G(s-j2\omega_1), G(s), \cdots \end{Bmatrix} \tag{2-20}$$

The closed-loop system of the converter under unbalanced grid conditions can be derived as Figure 2-14. The HTF of time delay is represented by $\mathbf{G}_d$. The HTF of the current controller is represented by $\mathbf{G}_i$. The plant models are represented by $\mathbf{Y}_o$ and $\mathbf{Y}_p$. Consequently, the output admittance model of the converter system can be derived as

$$\mathbf{Y}(s) = -\frac{\begin{bmatrix} \hat{\mathbf{i}} \\ e^{j2\theta^+}\hat{\mathbf{i}}^* \end{bmatrix}}{\begin{bmatrix} \hat{\mathbf{v}}^g \\ e^{j2\theta^+}\hat{\mathbf{v}}^{g*} \end{bmatrix}} = \left(\mathbf{I} + \mathbf{Y}_p\mathbf{G}_d\mathbf{G}_i\right)^{-1}\left(\mathbf{Y}_o - \mathbf{Y}_p\mathbf{G}_d\mathbf{G}_i\mathbf{Y}_{PLL}\right) \tag{2-21}$$

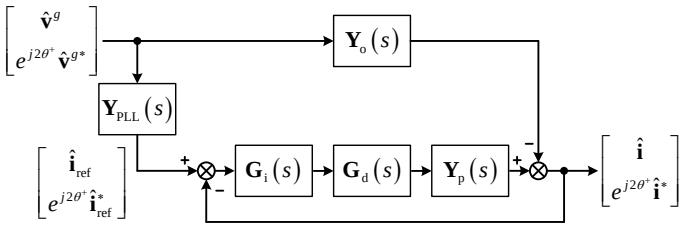

Figure 2-14 Closed-loop stationary-frame converter model in unbalanced grids. Source: [J2].

2.2.4. MODEL VALIDATION

The impedance measurement approach developed in the Section 2.1 can also be applied to validate model in unbalanced grid conditions. For simplicity, the grid-following converter is connected to an ideal grid, where the input voltage can be arbitrarily designed in simulation. When the perturbation at ω is injected in the first voltage vector, all the elements in the corresponding column of the admittance matrix can be measured by calculating the current responses over the voltage response.

The admittance models with different PLLs are validated by the frequency scan. The circuit and control parameters of the converter can be found in [J2]. For the SRF-PLL, the admittance model is derived with the truncation order k=2, resulting in a 10-by-10 admittance matrix. The 3rd column can be measured by frequency scan. The six dominant elements are plotted in Figure 2-15, where the solid lines denote the analytical model and the asterisks represent the measured result.

With the Notch-SRF-PLL, the model is validated under the same condition. Since the Notch-SRF-PLL benefits in the model truncation with k=1, the derived admittance model is a 6-by-6 matrix. The 2nd column of the admittance model is measured in Figure 2-16. Compared with Figure 2-15, it can be seen that the the frequency couplings caused by the unbalanced voltage trajectories have been largely mitigated by the Notch-SRF-PLL, which are indicated by blue and green lines whose magnitudes are lower.

2.2.5. SUMMARY

The converter model can be derived by HTFs considering the time periodicity introduced by unbalanced votlage trajectories. The HTF models can be derived in the complex space, yielding a multi-frequency impedance model in the stationary frame. Such a model can be seen as a unified model, which works for both balanced and unblanced grid conditions. The model can be also obtained by impedance measurement.

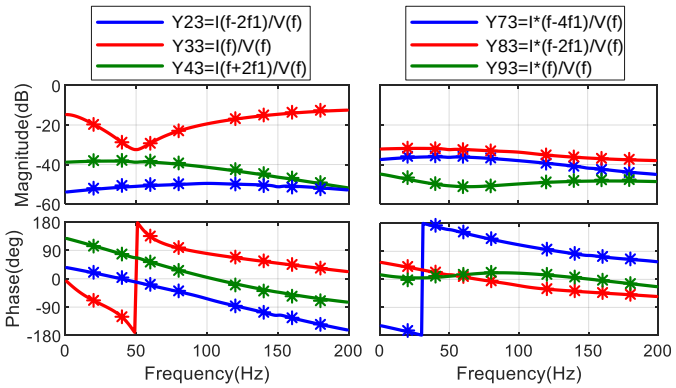

Figure 2-15 Admittance measurement of the converter with SRF-PLL. Source: [J2].

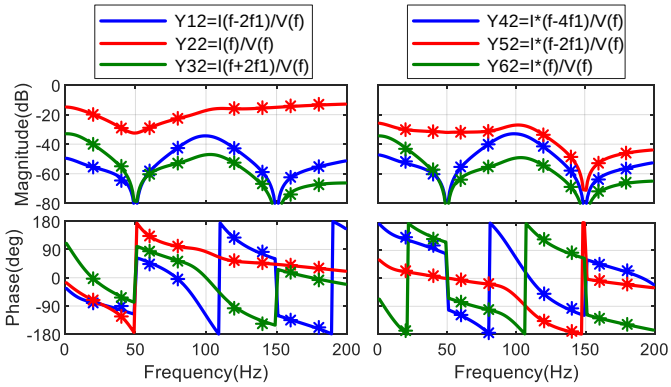

Figure 2-16 Admittance measurement of the converter with Notch-SRF-PLL. Source: [J2].

CHAPTER 3. IMPEDANE-BASED STABILITY ANALYSIS

"The hidden harmony is better than the obvious."

— Pablo Picasso

This chapter introduces the impedance-based stability analysis approaches for grid-interactive converter systems. First, the stability analysis approach based on SISO impedance models is proposed in Section 3.1 considering the existence of open-loop RHP poles. Then, the stability analysis based on MIMO impedance models is introduced in Section 3.2.

3.1. STABILITY ANALYSIS WITH SISO IMPEDANCE MODELS

The impedance-based stability analysis with SISO impedance models considering the open-loop RHP poles is proposed in this section, based on the content in the Publication [J3].

3.1.1. BACKGROUND

The stability of an interconnected converter system can be analyzed based on impedance modeling. The interconnected system can be partitioned as two subsystems at the point of common coupling (PCC). If the terminal impedances of these two subsystems at the PCC are known, the entire system dynamics can be analyzed based on the two impedance models. One alternative way is to regard the impedance ratio as the open-loop gain of the interconnected system and apply the NSC for stability assessment [13], [14]. Another way is to regard the impedance sum as the system characteristic equation, then the system stability can be predicted by analyzing its RHP zeros, which are the closed-loop unstable poles [41], [42].

The impedance-ratio-based stability method was firstly applied in 1970s in analyzing the stability of ac power systems [13]. In the power electronic fields, it was initially utilized for input filter design of dc-dc converters [14]. Since the impedance ratio can be straightforwardly separated as individual impedances for analysis on Bode diagrams, this method has been widely used for the design of dc converter systems, where the impedance profile of one subsystem can be specified to meet some stability requirements [18], [19].

However, these impedance specification methods assume that no open-loop RHP poles are present in the impedance ratio. Whenever the open-loop RHP poles exist, one has to plot the Nyquist diagram to consider the number of encirclements around

the critical point for stability analysis [37]. Therefore, to avoid RHP poles being present in the impedance ratio, it was suggested to define the impedance ratio according to the converter control types, by selecting the voltage-controlled converter systems (Type-Z) as the numerator impedance and the current-controller converter systems (Type-Y) as the denominator impedance [38], [39].

However, open-loop RHP pole issues may still be present in the impedance ratio for interconnected systems with two Type-Z systems [41], since the Type-Z system may have RHP zero in its terminal impedance. In such cases, the system stability can be judged by analyzing the locations of zeros in the impedance sum, since these zeros are the system closed-loop poles. Yet, the method also fails in the impedance specification, because the impedance sum cannot be separated into individual impedances for analysis.

It is seen that the above methods rely on a prior knowledge on the system types, which can be infeasible for "black-box" systems. Therefore, it is of interest to develop a more general impedance-based stability analysis approach which does not rely on the system types. This challenge is addressed in this section. An impedance-based stability analysis approach that allows for the existence of open-loop RHP poles and the impedance specifications on Bode diagrams is proposed.

3.1.2. IMPEDANCE-BASED STABILITY ANALYSIS APPROACH

The impedance-ratio-based stability analysis approach is studied. An interconnected system of two sources can be represented using the Thevenin's or Norton's equivalence, as shown in Figure 3-1. The voltages at the PCC in Figure 3-1(a) and Figure 3-1(b) can be derived, respectively, as

$$V = \frac{Z_2}{Z_1+Z_2}V_1 + \frac{Z_1}{Z_1+Z_2}V_2 = \frac{1}{1+\frac{Z_1}{Z_2}}V_1 + \frac{\frac{Z_1}{Z_2}}{1+\frac{Z_1}{Z_2}}V_2 = \frac{\frac{Z_2}{Z_1}}{1+\frac{Z_2}{Z_1}}V_1 + \frac{1}{1+\frac{Z_2}{Z_1}}V_2 \quad (3\text{-}1)$$

$$V = \frac{Z_1Z_2}{Z_1+Z_2}I_1 + \frac{Z_1Z_2}{Z_1+Z_2}I_2 = \frac{Z_1}{1+\frac{Z_1}{Z_2}}I_1 + \frac{Z_1}{1+\frac{Z_1}{Z_2}}I_2 = \frac{Z_2}{1+\frac{Z_2}{Z_1}}I_1 + \frac{Z_2}{1+\frac{Z_2}{Z_1}}I_2 \quad (3\text{-}2)$$

It is found that the impedance ratio, i.e., either Z_1/Z_2 or Z_2/Z_1, can be seen as an open-loop gain of the interconnected system. How to choose the appropriate impedance ratio for stability analysis will be studied.

A general approach is derived by rigorously mapping the NSC from the Nyquist diagram to the Bode diagram, which consists of the following four steps.

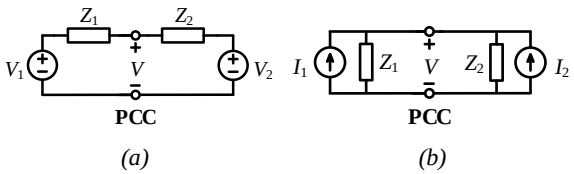

Figure 3-1 Impedanc-based representation of an interconnected system. (a) Thevenin's equivalence; (b) Norton's equivalence. Source: [J3].

3.1.2.1 Formulation of Impedance Ratio

The impedance ratio is seen as the open-loop gain for system stability analysis, therefore, it should be defined as a proper function, which is the assumption of the NSC [72]. The proper function requires that

$$\lim_{\omega\to\infty}\frac{Z_1(j\omega)}{Z_2(j\omega)}=0 \tag{3-3}$$

such that the impedance ratio finally goes into the unity circle on the Nyquist diagram. Then, its high-frequency response does not contribute to the encirclement around the critical point (−1, 0), which can be overlooked in the analysis.

Consequently, to make the impedance ratio proper, the high-frequency magnitude responses of Z_1 and Z_2 need to be compared:

- If they have different magnitude slopes in the high-frequency range, the numerator impedance should have the lower magnitude slope than the denominator impedance.
- If they have the same magnitude slopes in the high-frequency range, the numerator impedance should have the lower magnitude than the denominator impedance.

3.1.2.2 Identification of Open-Loop RHP Poles

The number of open-loop RHP poles in the impedance ratio can be calculated by

$$\boldsymbol{\mathcal{P}}[\boldsymbol{Z_1/Z_2}]=\boldsymbol{\mathcal{P}}[\boldsymbol{Z_1}]+\boldsymbol{\mathcal{Z}}[\boldsymbol{Z_2}] \tag{3-4}$$

where $\mathcal{P}$ represents the number of RHP poles and $\mathcal{Z}$ represents the number of RHP zeros. The Bode diagram allows for directly identifying the RHP poles and zeros based on the magnitude and phase changes. For an RHP pole, a magnitude slope

change of −20dB/dec with a corresponding phase change of +90° can be observed. For an RHP zero, a magnitude slope change of +20dB/dec with a corresponding phase change of −90° can be observed [36].

3.1.2.3 Identification of Encirclements

The number of encirclement of Z_1/Z_2 around the critical point on the Nyquist diagram can be judged on Bode diagrams of individual impedances. Figure 3-2 shows a mapping from the Nyquist diagram to the Bode diagram, which helps to identify the number of encirclements in the following way:

- On the Nyquist diagram, the number of encirclement is calculated as the crossing times of Z_1/Z_2 over the ray R. This is mapped to the number of phase crossings on the Bode diagram in the frequency range where $|Z_1| < |Z_2|$. Such a frequency range corresponds to the exterior region (ER) of the unity circle on the Nyquist diagram, thus is named as ER in figures for simplicity. The phase crossings are identified at the points where the difference between the two impedance phase curves is 180°, which are marked by red dots. To help identify the phase crossings on Bode diagram, one impedance phase curve is shifted of ±180° as the crossing boundaries (CBs). Then, the intersection of CBs and the other impedance phase curve is the phase crossing point.
- Then, by comparing the phase derivative relationship of the two impedances at each phase crossing point, the encirclement type can be determined. When the phase derivative of Z_1 is larger than that of Z_2, it is an anticlockwise crossing (ACC), and vice versa for the clockwise crossing (CC).
- Finally, the total number of encirclements can be calculated. It is noted that at any non-zero frequency, the number of encirclement should be doubled, since the encirclement for the negative frequency range is the same as that for the positive frequency range. But the encirclement at the zero frequency should be judged separately and should not be doubled [73].

3.1.2.4 Stability Prediction

With the known number of open-loop RHP poles and the total number of anticlockwise encirclements, the stability can be finally judged according to the NSC.

3.1.3. CASE STUDY

The proposed impedance-based stability analysis approach is used in a paralleled converter system for validation. The system configuration is shown in Figure 3-3, and the parameters can be found in [J3].

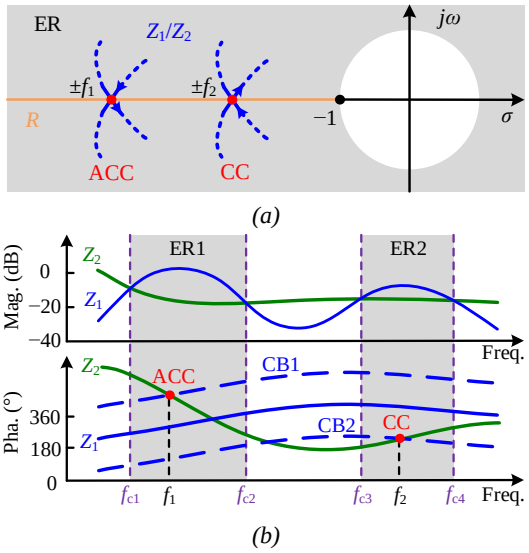

Figure 3-2 Impedanc-based stability analysis mapped from Nyquist diagram to Bode diagrams. (a) Nyquist diagram; (b) Bode diagram. Source: [J3].

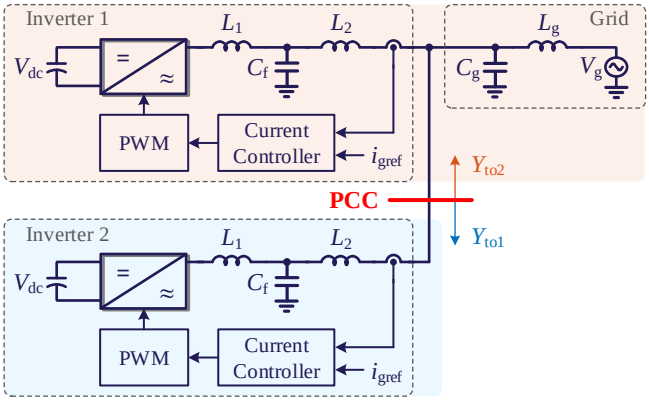

Figure 3-3 Studied paralleled converter system. Source: [J3].

Two converters are controlled as current sources, where their terminal admittance can be derived. The Inverter 1 is intentionally aggregated with the grid impedance, to ensure that the terminal admittance Y_{to2} has RHP zeros. Y_{to1} is the output admittance of Inverter 2.

The stability analysis by the proposed approach and the NSC are provided in Figure 3-4 and Figure 3-5, respectively. It can be observed that $|Y_{to2}|>|Y_{to1}|$ for the high-frequency response, such that Y_{to1}/Y_{to2} needs to be chosen as the open-loop gain. Two

RHP zeros are identified at f_r in Y_{to2} because of the phase jump of 180° at the anti-resonant point, indicating two open-loop RHP poles, which agrees with the pole-zero analysis result in Figure 3-5(a). In the frequency range where $|Y_{to1}| > |Y_{to2}|$, as shown in the shaded areas, there is no phase crossings, which agrees with the Nyquist diagram in Figure 3-5(b). Therefore, the system is unstable under this case (Case A), which is verified by experimental results given in Figure 3-6.

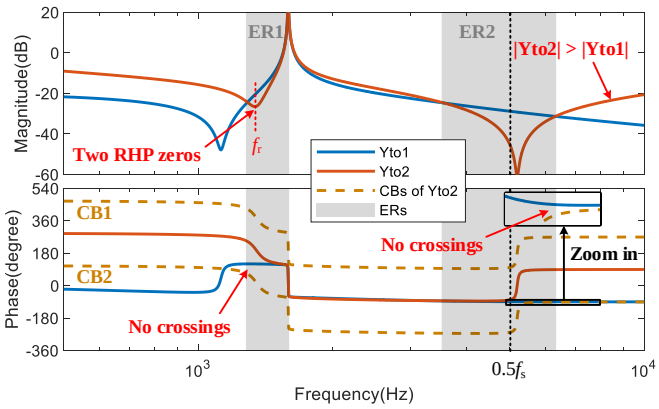

Figure 3-4 Stability analysis by the proposed approach. Source: [J3].

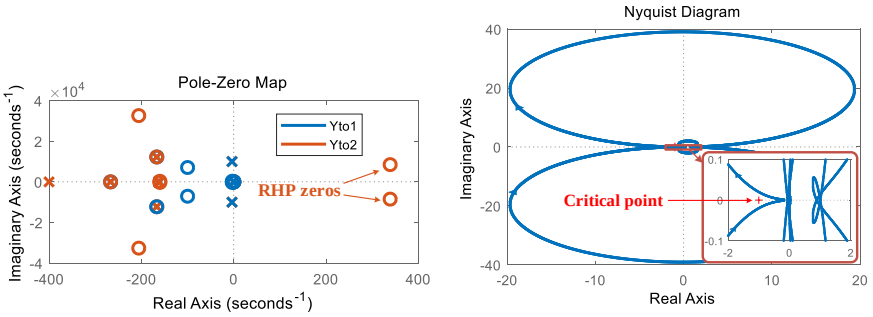

(a) *(b)*

Figure 3-5 Stability analysis by the NSC. (a) Pole-zero map; (b) Nyquist diagram of Y_{to1}/Y_{to2}. Source: [J3].

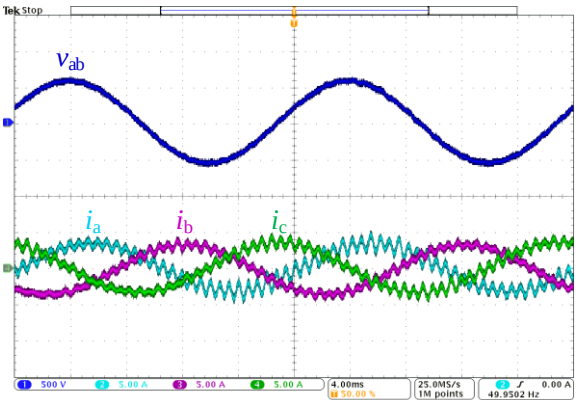

Figure 3-6 Experimental result for Case A. Source: [J3].

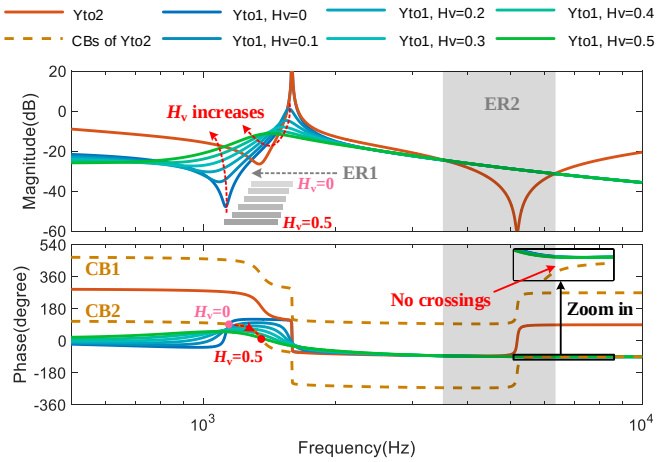

Figure 3-7 Impedance specification with open-loop RHP poles. Source: [J3].

Another case study (Case B) is performed to prove that the proposed approach can be utilized for impedance specification. The feedforward control parameter (H_v) of Inverter 2 is changed to modify the impedance profile of Y_{to1}, such that the number of ACCs can be equal to the number of open-loop RHP poles for the system stabilization. Such impedance specification can be done by the Bode-diagram analysis on Figure 3-7, whose stabilization effect is verified by the experimental result in Figure 3-8.

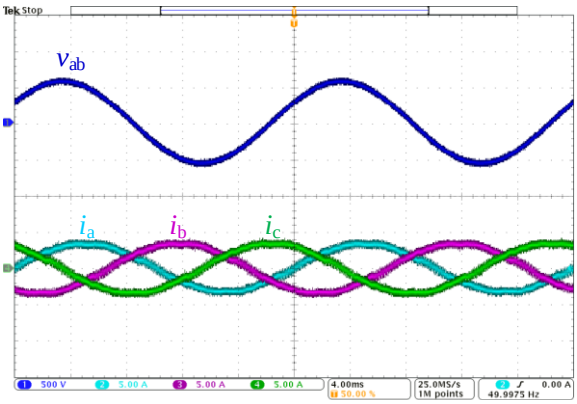

Figure 3-8 Experimental result for Case B with H_v=0.5. Source: [J3].

3.2. STABILITY ANALYSIS WITH MIMO IMPEDANCE MODELS

Considering the low-frequency control dynamics of converter systems, the impedance models are characterized by MIMO matrices. The stability analysis methods for MIMO systems are introduced in this section. The case studies are provided based on the content in the Publication [J2].

3.2.1. MIMO STABILITY ANALYSIS APPROACHES

Similar to the stability analysis for SISO systems, the stability analysis for MIMO systems can also be performed based on open-loop gain analysis and closed-loop pole analysis.

3.2.1.1 Open-Loop Gain Analysis Approach

For MIMO systems, the impedance ratio is represented by a matrix, which is defined as **L**. Then, the generalized NSC [35] can be applied for stability analysis. The stability is assessed by the eigenvalues of the open-loop gain matrix, i.e.,

$$\det\left(\lambda\mathbf{I}-\mathbf{L}\right)=0\Rightarrow\lambda_i\left(\mathbf{L}\right) \tag{3-5}$$

The system is stable if and only if each eigenvalue satisfies the NSC. Since each eigenvalue is a SISO transfer function, the generalized NSC actually analyzes the stability by decoupling the original MIMO system into multiple decoupled SISO systems. Then, the frequency-domain analysis approaches for SISO systems can be applied to each eigenvalue transfer function.

3.2.1.2 Closed-Loop Pole Analysis Approach

In addition to the open-loop gain analysis, the stability of a MIMO system can also be analyzed by the closed-loop poles. This is equivalent to analyzing the zeros of the characteristic equation, by solving

$$\det\left(\mathbf{I}+\mathbf{L}\right)=0 \tag{3-6}$$

If there are RHP zeros in (3-6), the system is closed-loop unstable. Sometimes, the system characteristic equation can be represented as the impedance sum [41]. The zero location analysis can be simply conducted on the Bode diagram of det(**I**+**L**), as introduced in Section 3.1.2.2. It can be seen that det(**I**+**L**) is a SISO transfer function. Thus, this method also analyzes the MIMO system stability using an equivalent SISO model.

3.2.2. CASE STUDY

The above two analysis approaches are applied for stability analysis of a grid-following converter in unbalanced grids. Figure 3-9 shows the studied system. The grid impedance (L_{ga}, L_{gb} and L_{gc}) is unbalanced.

For stability analysis, the converter output admittance $\mathbf{Y}(s)$ is modeled as a six-by-six matrix according to (2-21). The grid impedance $\mathbf{Z}_g(s)$ can be derived based on symmetrical component decomposition [74], and then extended into a higher-order matrix considering the same frequency-coupling relationships of the converter impedance.

Assuming a three-phase unbalanced impedance as $Z_a(s)$, $Z_b(s)$, and $Z_c(s)$ for each phase, the impedance in sequence domain can be firstly derived by the symmetrical component decomposition as

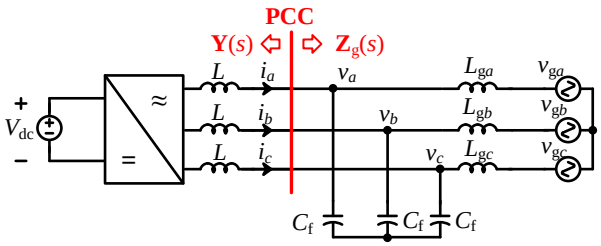

Figure 3-9 A grid-following converter connected to unbalanced grids. Source: [J2].

$$\begin{bmatrix} \mathbf{V}(s) \\ \mathbf{V}^*(s) \end{bmatrix} = \frac{1}{3}\begin{bmatrix} Z_{11}(s) & Z_{12}(s) \\ Z_{21}(s) & Z_{22}(s) \end{bmatrix}\begin{bmatrix} \mathbf{I}(s) \\ \mathbf{I}^*(s) \end{bmatrix} \tag{3-7}$$

where $Z_{11}(s)=Z_{22}(s)=Z_a(s)+Z_b(s)+Z_c(s)$, $Z_{12}(s)=Z_a(s)+a^2Z_b(s)+aZ_c(s)$, $Z_{21}(s)=Z_a(s)+aZ_b(s)+a^2Z_c(s)$, given $a=e^{j2\pi/3}$. Then, considering the same matrix size of $\mathbf{Y}(s)$, (3-7) can be extended into a higher-order matrix as

$$\mathbf{Z}(s)=\frac{1}{3}\begin{bmatrix} Z_{11}(s-j2\omega_1) & & & & Z_{12}(s-j2\omega_1) & \\ & Z_{11}(s) & & & & Z_{12}(s) \\ & & Z_{11}(s+j2\omega_1) & & & \\ & & & Z_{22}(s-j4\omega_1) & & \\ Z_{21}(s-j2\omega_1) & & & & Z_{22}(s-j2\omega_1) & \\ & Z_{21}(s) & & & & Z_{22}(s) \end{bmatrix} \tag{3-8}$$

A critically unstable case of the grid-connected converter system is studied, where the parameters can be found in [J2]. The stability analysis results are provided in Figure 3-10 and Figure 3-11. In Figure 3-10, only four of the six eigenvalues are shown in a zoomed-in figure. It can be seen that λ_1 and λ_2 critically encircle (−1,0) on the complex plane, indicating unstable. In Figure 3-11, four RHP zeros can be identified.

The simulation validation is provided in Figure 3-12. According to the discrete Fourier analysis of the phase-*a* current, it is found that the system oscillation frequencies have been accurately predicted by the RHP zero analysis in Figure 3-11.

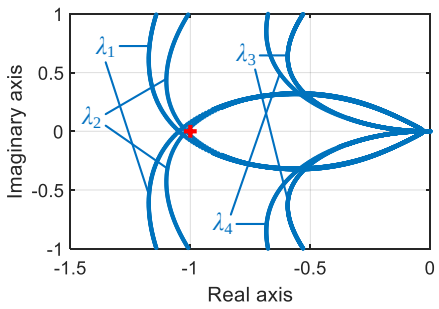

Figure 3-10 Stability analysis by the generalized NSC. Source: [J2].

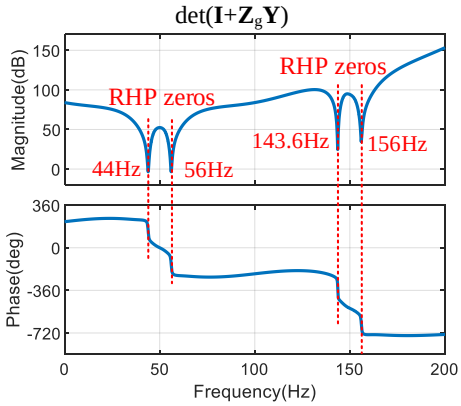

Figure 3-11 Stability analysis by the characteristic equation. Source: [J2].

3.3. SUMMARY

The impedance-based stability analysis approaches for SISO and MIMO systems have been studied in this chapter.

- For SISO systems, the stability analysis based on impedance ratios can be implemented on Bode diagrams of individual impedances, even with the existence of open-loop RHP poles.
- For MIMO systems, the generalized NSC or the characteristic-equation-based method transforms the original MIMO system into SISO systems. Consequently, the stability analysis approaches developed for SISO systems can still be applied.

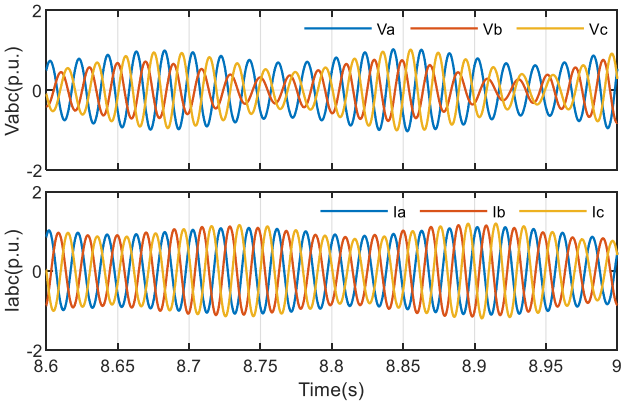

(a)

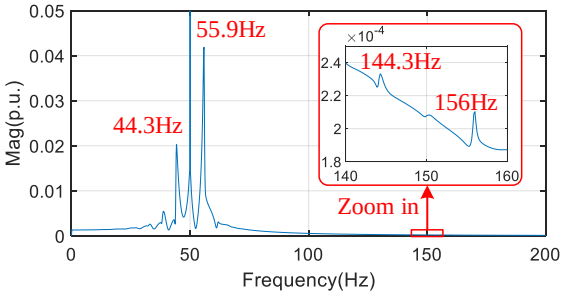

(b)

Figure 3-12 Simulation validation for the grid-connected converter. (a) Time-domain waveforms; (b) discrete Fourier analysis of the phase-a current. Source: [J2].

CHAPTER 4. CONTROL DESIGN OF GRID-FORMING CONVERTERS

"Simplicity is the ultimate sophistication."

— Leonardo da Vinci

This chapter applies the developed impedance modeling and stability analysis approaches to grid-forming converters, in order to perform control design for stability enhancement. Section 4.1 studies the impedance passivity impacted by the voltage control loop of grid-forming converters. A passivity-based control co-design method is proposed. Section 4.2 studies the low-frequency stability of grid-forming converters by proposing an impedance decomposition method, which can characterize different control-loop impacts on the closed-loop output impedance and thus benefit to a design-oriented analysis.

4.1. PASSIVITY ANSLYSIS OF GRID-FORMING CONVERTERS

The passivity analysis of grid-forming converter is studied in this section by the impedance-based analysis. A controller co-design approach for voltage loop of grid-forming converters is proposed, which achieves the impedance passivity till half of the sampling frequency for stability enhancement. The content is based on the Publication [J4].

4.1.1. BACKGROUND

The grid-forming converters can adopt various voltage control schemes. These control schemes can be in general classified into the single-loop control [75], [76] and dual-loop control [77]-[80], as shown in Figure 4-1. Their control performances considering voltage unbalance and harmonic distortions have been discussed for a long time. However, there are only a few works focusing on their impacts on the output impedance passivity.

The passivity of the converter output impedance is important to the converter-grid interaction. If the converter has negative output impedance, it can interact with grid impedances and lead to some harmonic instability issues [19]. The passivity-based analysis and control has been studied a lot on grid-following converters [46]-[48], [81], [82]. However, these findings and stability enhancement solutions cannot be readily applied to grid-forming converters, since the plants and control structures are different.

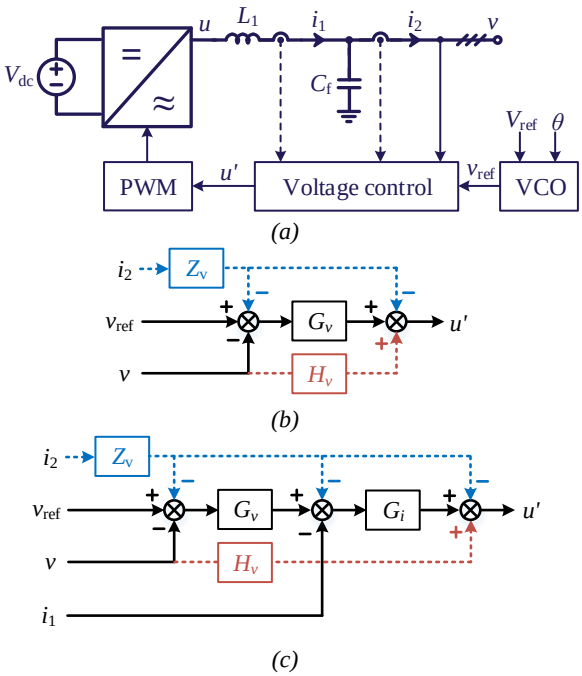

Figure 4-1 Control schemes for grid-forming converter. (a) Circuit diagram; (b) Single-loop control; (c) Dual-loop control. Source: [J4].

For the grid-forming converters, there only two recent works focusing the passivity analysis [83], [84]. A passivity-oriented control is proposed in [83], yet the analysis is based on modeling in the discrete domain, which can hardly provide a design-oriented analysis. In [84], a passivity-based control is proposed based on the continuous-domain modeling and analysis, yet it is only based on a specific control scheme. How the passivity analysis applied to other voltage control schemes are still unclear.

To fill in the research gap, the passivity of grid-forming converters is studied in this section. The frequency-domain impedance passivity analysis of grid-forming converters with different voltage control schemes is studied. Then, a passivity-based controller co-design approach is proposed, which enables to achieve passivity till half of the sampling frequency. The control performance is finally validated by the stability analysis of grid-connected converters.

4.1.2. PASSIVITY ANALYSIS

The impedance passivity is studied based on the closed-loop impedance model. For single-loop control and dual-loop control, the impedance model are derived as:

$$Z_o = -\frac{v}{i_2} = \frac{Z_{ol} + G_{uv}G_dZ_v}{1+T_1+T_2} \quad \text{for single-loop control} \tag{4-1}$$

$$Z_o = -\frac{v}{i_2} = \frac{Z_{ol}(1+T_2) + G_{uv}G_dG_iG_{ii} + G_{uv}G_dG_iZ_v}{1+T_1+T_2+T_3} \quad \text{for dual-loop control} \tag{4-2}$$

where the transfer functions can be derived from the small-signal model shown in Figure 4-2. Z_{ol}, G_{uv}, G_{ii} and G_{ui} are open-loop plant models [85]. G_v and G_i are transfer functions of the voltage and current controllers. G_d is the time delay. H_v is the feedback decoupling loop and Z_v is the virtual impedance control, which are optional.

Since the virtual impedance control is designed in the feedforward loop, it only affect the output impedance yet without impacting the voltage control loop gain. Thus, the virtual impedance control can be designed to improve the impedance passivity.

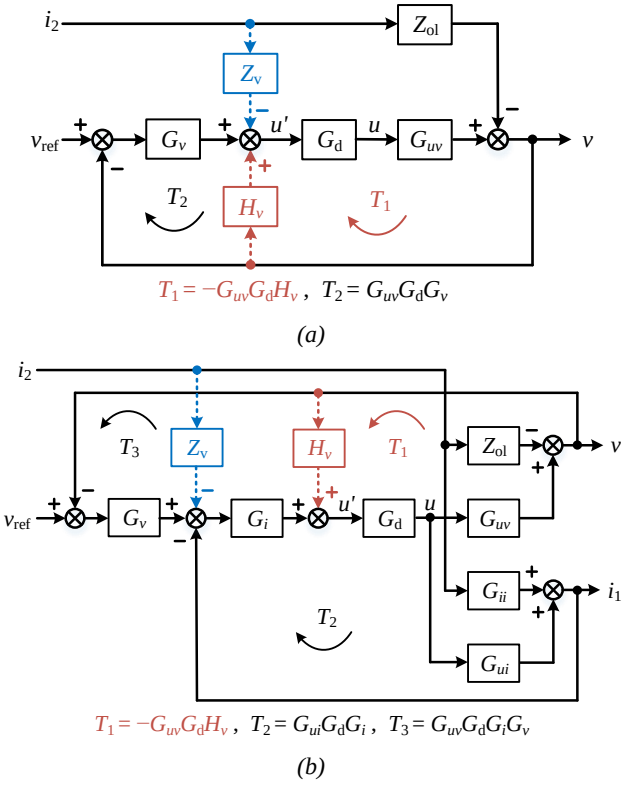

Figure 4-2 Small-signal model of grid-forming converter. (a) Single-loop control; (b) Dual-loop control. Source: [J4].

4.1.2.1 Single-Loop Control

For the single-loop control, assuming $G_v \approx K_P+K_I/s$ for the high-frequency response, then the sign of the real part of the converter output impedance can be derived as

$$\operatorname{sgn}\left\{R_o(\omega)\right\}=\operatorname{sgn}\left\{-K_P\omega L_1\sin(\omega T_d)-K_I L_1\cos(\omega T_d)\right\} \tag{4-3}$$

It is seen that if K_P=0, i.e., the converter adopts a high-frequency integral-dominant (I-dominant) controller [76], [85], the sign of R_o is merely determined by the sign of $\cos(\omega T_d)$, which simplifies the passivity analysis. The resultant negative resistance is within the low-frequency range where $f < f_c=1/(4T_d)$.

If further considering the virtual impedance control (Z_v) based on a high-frequency I-dominant voltage controller, the sign of R_o can be derived as

$$\operatorname{sgn}\left\{R_o(\omega)\right\}=\operatorname{sgn}\left\{\left[Z_v\left(1-\omega^2 L_1 C_f\right)-K_I L_1\right]\cos(\omega T_d)\right\} \tag{4-4}$$

It can be seen that Z_v influences the coefficient of $\cos(\omega T_d)$. If this coefficient can be designed with the same sign as $\cos(\omega T_d)$, the positive output resistance can be realized. This leads to the condition of

$$Z_v=\frac{K_I L_1}{1-\omega_c^2 L_1 C_f}=\frac{K_I L_1}{1-\left(\frac{\pi}{2T_d}\right)^2 L_1 C_f}>0 \tag{4-5}$$

which guarantees that the converter has non-negative resistance till half of the sampling frequency.

4.1.2.2 Dual-Loop Control

For the dual-loop control, assuming $G_v \approx K_P+K_I/s$ and $G_i \approx K_{pi}$ for the high-frequency response approximation, the frequency range of the negative resistance can be indicated by

$$\operatorname{sgn}\left\{R_o(\omega)\right\}=\operatorname{sgn}\left\{-\omega L_1 K_{pi} K_P\sin(\omega T_d)+K_{pi}\left(1-K_I L_1\right)\cos(\omega T_d)+K_{pi}^2 K_P\right\} \tag{4-6}$$

It is seen that when K_P=0, i.e., a high-frequency I-dominant voltage controller is used, the frequency range of the negative resistance is only related to the sign of $\cos(\omega T_d)$. Differing from the case of single-loop control, it is found that the dual-loop control results in the negative resistance in a higher frequency range of (f_c, f_s/2).

Similarly, if the virtual impedance control (Z_v) is considered with the high-frequency I-dominant voltage controller, it can be derived that

$$\operatorname{sgn}\left\{R_o\left(\omega\right)\right\}=\operatorname{sgn}\left\{K_{pi}\left[1-K_I L_1+Z_v\left(1-\omega^2 L_1 C_f\right)\right]\cos\left(\omega T_d\right)\right\} \tag{4-7}$$

which yields the passivity condition below f_s/2 as

$$Z_v=\frac{1-K_I L_1}{\omega_c^2 L_1 C_f-1}=\frac{1-K_I L_1}{\left(\frac{\pi}{2T_d}\right)^2 L_1 C_f-1}>0 \tag{4-8}$$

Based on the dual-loop control structure, if the voltage feedback decoupling loop (H_v) is further considered, assuming $G_v \approx K_P+K_I/s$ and considering Z_v, the sign of R_o can be derived as

$$\operatorname{sgn}\left\{R_o\right\}=\operatorname{sgn}\left\{\begin{array}{l}-\omega L_1\left(K_{pi}K_P-H_v\right)\sin\left(\omega T_d\right)\\ +K_{pi}\left[1-K_I L_1+Z_v\left(1-\omega^2 L_1 C_f\right)\right]\cos\left(\omega T_d\right)\\ +K_{pi}\left(1+Z_v\right)\left(K_{pi}K_P-H_v\right)\end{array}\right\} \tag{4-9}$$

It can be seen that, the feedback decoupling loop needs to be co-designed with the voltage and current controller to satisfy $K_{pi}K_P - H_v = 0$, such that the sign of R_o is only related to the term with $\cos(\omega T_d)$. The coefficient of $\cos(\omega T_d)$ is the same as that in (4-7), thus the passivity-based control design can be realized by the same condition shown in (4-8).

4.1.3. VALIDATION

The previous impedance passivity analysis and the passivity-based control co-design approach are validated in both frequency and time domains.

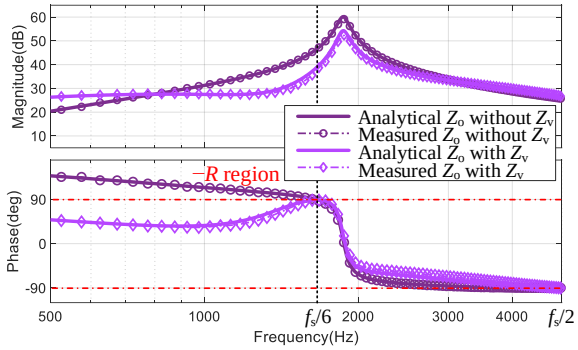

Figure 4-3 Impedance measurement for single-loop control (Case I). Source: [J4].

4.1.3.1 Frequency-Domain Validation

The converter impedance passivity is firstly validated by the impedance measurement in the frequency domain. The impedance measurement results for three cases are shown in Figure 4-3, Figure 4-4, and Figure 4-5. The three cases adopts different control schemes:

- Case I: single-loop control with high-frequency I-dominant voltage controller;
- Case II: dual-loop control with high-frequency I-dominant voltage controller;
- Case III: dual-loop control with voltage feedback decoupling loop, where the voltage feedback decoupling controller is co-designed with the voltage and current controllers by satisfying $K_{pi}K_P - H_v = 0$.

It can be seen that for the single-loop control, the negative resistance is in the frequency range lower than the critical frequency f_c=f_s/6. When the virtual impedance control is enabled, the passive region is widen to half of the sampling frequency f_s/2. For the dual-loop control, the negative resistance is within (f_c, f_s/2), which can be also compensated by the virtual impedance control. These analysis results agree with the previous theoretical derivations.

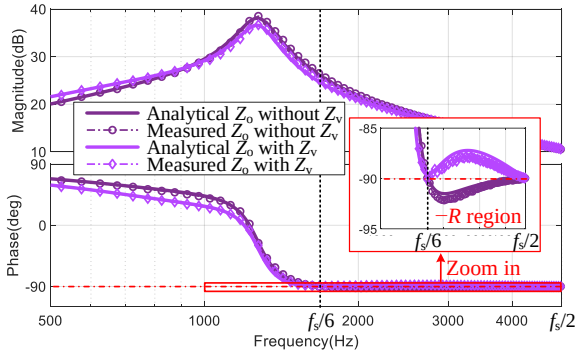

Figure 4-4 Impedance measurement for dual-loop control (Case II). Source: [J4].

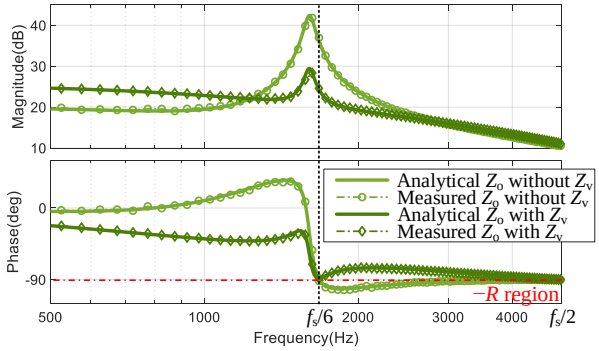

Figure 4-5 Impedance measurement for dual-loop control with voltage feedback decoupling (Case III). Source: [J4].

4.1.3.2 Time-Domain Validation

The time-domain validation is then performed for the stability analysis of grid-forming converters. Two cases are tested by experiments, as shown in Figure 4-6:

- Case A: single-loop control with a resonant grid;
- Case B: dual-loop control with an inductive grid.

For Case A, the impedance-based stability analysis and experimental validation are provided in Figure 4-7. From the impedance Bode diagrams, it is seen that the negative resistance of Z_o is introduced below $f_s/6$ without Z_v, which leads to the impedance phase difference larger than 180° at the impedance magnitude crossover frequency. Thus, the instability occurs. Such instability can be mitigated by the enabling the virtual impedance control. The experimental result shows the same phenomenon.

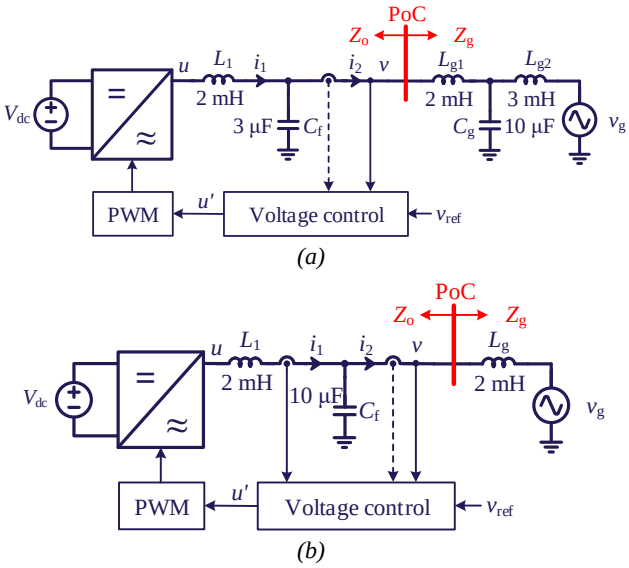

Figure 4-6 Two cases for the experimental validations of harmonic stability of grid-forming converters. (a) Single-loop control with a resonant grid (Case A); (b) dual-loop control with an inductive grid (Case B). Source: [J4].

For Case B, the stability analysis and experimental validation are provided in Figure 4-8, which verify the same active damping effect by the virtual impedance control for the dual-loop voltage control.

4.1.4. SUMMARY

The impedance passivity impacted by the voltage control of grid-forming converters is studied in this section. It is found that:

- The non-passive frequency range for grid-forming converters is impacted by time delay and the voltage control schemes. For single-loop control, the non-passive region is present in a lower frequency range, while for the dual-loop control, it is present in a higher frequency range.
- The virtual impedance co-designed with other controller loops can achieve the impedance passivity till half of the sampling frequency, which improves the stability of grid-forming converter in grid-connected applications.

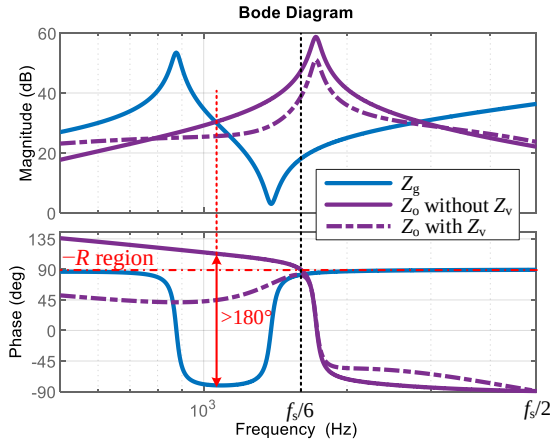

(a)

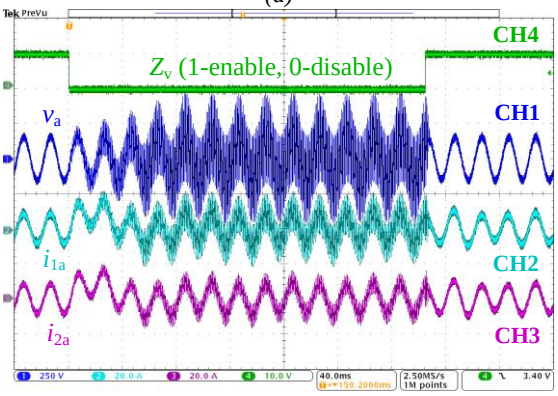

(b)

Figure 4-7 Impedance-based stability analysis and experimental validation for Case A. (a) Impedance-based stability analysis; (b) Experimental waveforms. Source: [J4].

4.2. CONTROL-LOOP IMPACT ANALYSIS OF GRID-FORMING CONVERTERS

The low-frequency stability of grid-forming converters is studied in this section based on the impedance modeling and analysis. An impedance decomposition approach is proposed to characterize different control-loop impacts, which clarifies how the control loops affect the impedance shaping and further impact the converter-grid interaction. The content is based on the Publication [J5].

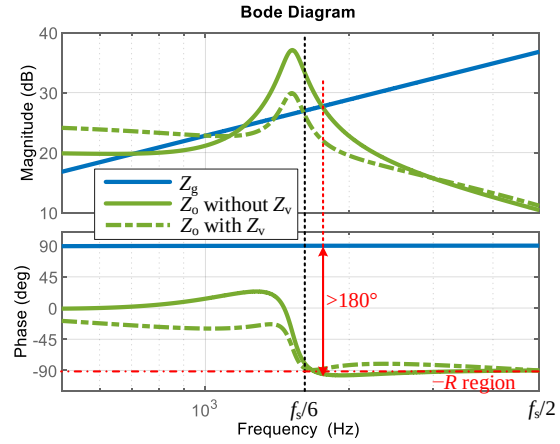

(a)

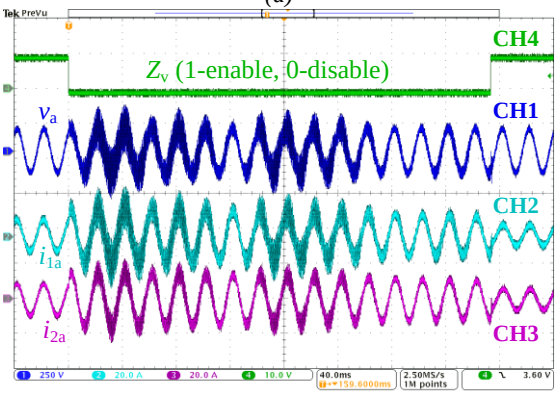

(b)

Figure 4-8 Impedance-based stability analysis and experimental validation for Case B. (a) Impedance-based stability analysis; (b) Experimental waveforms. Source: [J4].

4.2.1. BACKGROUND

The grid-forming converters have become more and more popular in recent years, since they can provide superior stability than grid-forming converters in weak grids [54]-[57]. However, they may also suffer from instability issues in stiff grids [5], [58]. Therefore, the dynamic modeling and stability analysis for grid-forming converters in grid-connected applications are also important.

The state-space analysis and impedance-based analysis have been applied for the dynamic studies of grid-forming converters. The state-space analysis is based on the eigenvalue analysis of the system state matrix. The participation factor and parametric sensitivity analysis can be then performed to investigate how specific state variables or parameters affect the system oscillation modes [59], [60]. The impedance-based

stability analysis is based on the generalized NSC, since the converter impedance is modeled as a MIMO system in the frequency domain [61], [62].

Although both state-space analysis with eigenvalues and impedance-based analysis with the generalized NSC can analyze how different control parameters affect the system stability, it is still unclear to understand the interaction of different control loops, since the eigenvalues of the state space model or the eigenvalue transfer functions of the impedance ratio matrix have to be calculated numerically. These numerical-based studies make it hard to reveal the stabilizing or destabilizing mechanism of converter control loops.

To tackle this challenge, an impedance decomposition method for grid-forming converters is proposed, which enables to characterize the impact of different control loops on the impedance shaping. Consequently, the magnitude analysis based on Bode diagrams can be used to identify the impacts of different control loops in the frequency domain. Such a decomposition also benefits to the controller design for stability enhancement of grid-forming converters in stiff grids.

4.2.2. IMPEDANCE MODELING AND DECOMPOSITION

A droop-controlled grid-forming converter is studied in this work as the example for the converter modeling. The circuit and control diagrams are shown in Figure 4-9. The outer loop adopts the typical droop control for the power synchronization. The inner loop adopts the basic dual-loop control as introduced in Section 4.1.

The frequency-domain model of the grid-forming converter is derived in the complex $\alpha\beta$ frame [86], which is shown in Figure 4-10.

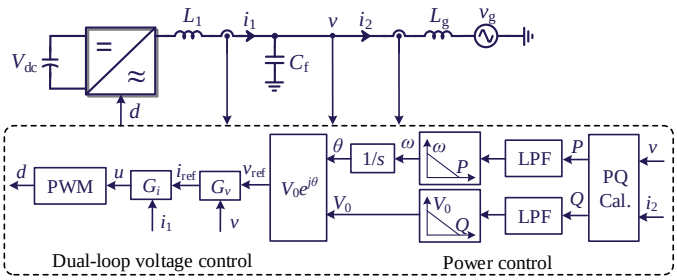

Figure 4-9 Droop-controlled grid-forming converter in grid connection. Source: [J5].

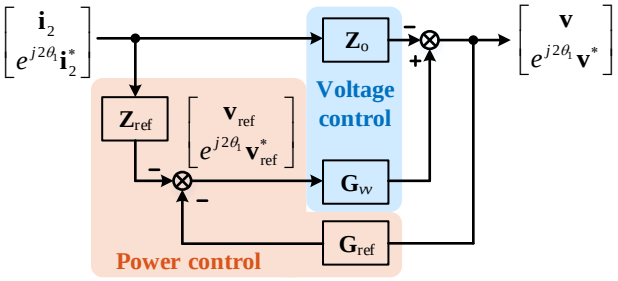

Figure 4-10 Small-signal model of the grid-forming converter in complex $\alpha\beta$ frame. Source: [J5].

In Figure 4-10, $\mathbf{Z}_o$ and $\mathbf{G}_{vv}$ are frequency-shifted transfer function matrices of the voltage control loop, given by

$$\mathbf{Z}_o = \begin{bmatrix} Z_o(s) & 0 \\ 0 & Z_o(s-j2\omega_1) \end{bmatrix} \tag{4-10}$$

$$\mathbf{G}_{vv} = \begin{bmatrix} G_{vv}(s) & 0 \\ 0 & G_{vv}(s-j2\omega_1) \end{bmatrix} \tag{4-11}$$

where $Z_o(s)$ and $G_{vv}(s)$ are the closed-loop output impedance and the voltage transfer function derived based on Figure 4-2(b).

$\mathbf{Z}_{ref}$ and $\mathbf{G}_{ref}$ are derived based on linearization of the power control loop, given by

$$\mathbf{Z}_{ref} = \frac{j}{2}\begin{bmatrix} -\left(V_0G_P(s-j\omega_1)+G_Q(s-j\omega_1)\right)V_{dq}^* & -\left(V_0G_P(s-j\omega_1)-G_Q(s-j\omega_1)\right)V_{dq} \\ \left(V_0G_P(s-j\omega_1)-G_Q(s-j\omega_1)\right)V_{dq}^* & \left(V_0G_P(s-j\omega_1)+G_Q(s-j\omega_1)\right)V_{dq} \end{bmatrix} \tag{4-12}$$

$$\mathbf{G}_{ref} = \frac{j}{2}\begin{bmatrix} -\left(V_0G_P(s-j\omega_1)-G_Q(s-j\omega_1)\right)I_{2dq}^* & -\left(V_0G_P(s-j\omega_1)+G_Q(s-j\omega_1)\right)I_{2dq} \\ \left(V_0G_P(s-j\omega_1)+G_Q(s-j\omega_1)\right)I_{2dq}^* & \left(V_0G_P(s-j\omega_1)-G_Q(s-j\omega_1)\right)I_{2dq} \end{bmatrix} \tag{4-13}$$

where $G_P(s)$ and $G_Q(s)$ are determined by the transfer functions of the active and reactive power loops, respectively. V_0 is the voltage magnitude, and I_{2dq} is the output current in the voltage dq frame.

Based on Figure 4-10, the impacts of the active and reactive power control loops can be further decomposed into different feedforward loops, yielding the model in Figure 4-11(a). Thus, the output impedance model of the grid-forming converter can be

represented by a series connection of different control impedances, as shown in Figure 4-11(b), i.e.,

$$\mathbf{Z}_{\mathrm{VSC}} = \underbrace{\left(\mathbf{I}+\mathbf{G}_{vv}\mathbf{G}_{\mathrm{ref}}\right)^{-1}\mathbf{Z}_{\mathrm{o}}}_{\mathbf{Z}_{\mathrm{VC}}} + \underbrace{\left(\mathbf{I}+\mathbf{G}_{vv}\mathbf{G}_{\mathrm{ref}}\right)^{-1}\mathbf{G}_{vv}\mathbf{Z}_{\mathrm{refP}}}_{\mathbf{Z}_{\mathrm{APC}}} + \underbrace{\left(\mathbf{I}+\mathbf{G}_{vv}\mathbf{G}_{\mathrm{ref}}\right)^{-1}\mathbf{G}_{vv}\mathbf{Z}_{\mathrm{refQ}}}_{\mathbf{Z}_{\mathrm{RPC}}} \tag{4-14}$$

where VC means the voltage control, APC means the active power control, and RPC means the reactive power control. $\mathbf{Z}_{\mathrm{refP}}$ and $\mathbf{Z}_{\mathrm{refQ}}$ can be separated from (4-12) as

$$\mathbf{Z}_{\mathrm{refP}} = \frac{j}{2}\begin{bmatrix} -V_0 G_P\left(s-j\omega_1\right)V_{dq}^{*} & -V_0 G_P\left(s-j\omega_1\right)V_{dq} \\ V_0 G_P\left(s-j\omega_1\right)V_{dq}^{*} & V_0 G_P\left(s-j\omega_1\right)V_{dq} \end{bmatrix} \tag{4-15}$$

$$\mathbf{Z}_{\mathrm{refQ}} = \frac{j}{2}\begin{bmatrix} -G_Q\left(s-j\omega_1\right)V_{dq}^{*} & G_Q\left(s-j\omega_1\right)V_{dq} \\ -G_Q\left(s-j\omega_1\right)V_{dq}^{*} & G_Q\left(s-j\omega_1\right)V_{dq} \end{bmatrix} \tag{4-16}$$

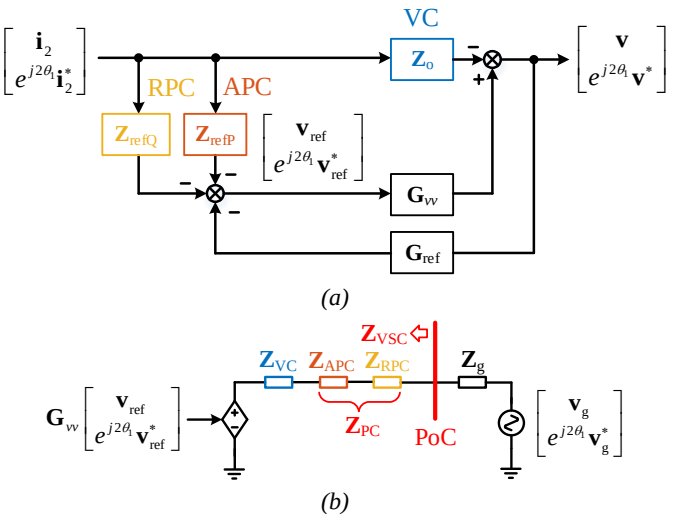

Figure 4-11 Impedance decomposition based on control loops. (a) Feedforward loop decomposition; (b) Equivalent circuit. Source: [J5].

In (4-14), $\mathbf{G}_{vv}$ and $\mathbf{G}_{\mathrm{ref}}$ appear in the feedback loop. They do not contribute to the differences in the decomposed impedances. The differentiated impacts of the three control loops are originated from $\mathbf{Z}_{\mathrm{o}}$, $\mathbf{Z}_{\mathrm{refP}}$ and $\mathbf{Z}_{\mathrm{refQ}}$, since $\mathbf{G}_{vv}$ can be approximated as

an identity matrix within the bandwidth of the voltage control loop. Therefore, the impedance shaping effects impacted by the three control loops can be compared on the Bode diagrams of the decomposed impedances, which can help conduct a design-oriented analysis for stability of grid-forming converters in grid connections.

4.2.3. CASE STUDY

The stability of the grid-forming converter is analyzed based on the impedance decomposition. The instability mechanism of the grid-forming converter in stiff grids is firstly studied by the impedance-based analysis. Then, how the impedance decomposition can guide the controller design is introduced.

4.2.3.1 Instability Mechanism in Stiff Grids

The generalized NSC is applied to the impedance ratio $\mathbf{L} = \mathbf{Z}_{\text{VSC}}\mathbf{Z}_{\text{g}}^{-1}$ for the stability analysis. According to the small-gain theorem, if each eigenvalue of $\mathbf{L}$ (λ_i) is less than 0 dB, the system is always stable [87]. Since the converter output impedance $\mathbf{Z}_{\text{VSC}}$ is non-passive in the low-frequency range due to the constant power control effect, the phase of λ_i can inevitably cross over 180° in the low-frequency range. Thus, the stability tends to be worse if the frequency range for $\lambda_i > 0$ dB is wider.

It is known that the magnitude of λ_i is bounded by

$$\left|\lambda_i\left(\mathbf{L}\right)\right| \le \bar{\sigma}\left(\mathbf{Z}_{\text{VSC}}\right)\bar{\sigma}\left(\mathbf{Z}_{\text{g}}^{-1}\right) = \bar{\sigma}\left(\mathbf{Z}_{\text{VSC}}\right)/\underline{\sigma}\left(\mathbf{Z}_{\text{g}}\right) \tag{4-17}$$

where $\bar{\sigma}(\bullet)$ is the maximum singular value and $\underline{\sigma}(\bullet)$ is the minimum singular value. Therefore, the singular value analysis of $\mathbf{Z}_{\text{VSC}}$ and $\mathbf{Z}_{\text{g}}$ can explain why the instability tends to happen with grid-forming converters in stiff grids.

Figure 4-12 shows the generalized NSC analysis under different short circuit ratios (SCRs). The passivity index ($p_{\min}$) [50] is also plotted in the figure, since the phase crossover frequencies of the eigenvalues of $\mathbf{L}$ are always in the non-passive region of the converter system [87]. For SCR = 10, it can be seen that a RHP pole exist at 50 Hz in λ_1, which can be compensated by the anticlockwise crossing (ACC). At the two clockwise crossings (CCs), the eigenvalue λ_1 is critically larger than 0 dB, indicating a critically unstable system. For SCR=7, the eigenvalue λ_1 becomes less than 0 dB at the two CCs, thus the system becomes stable.

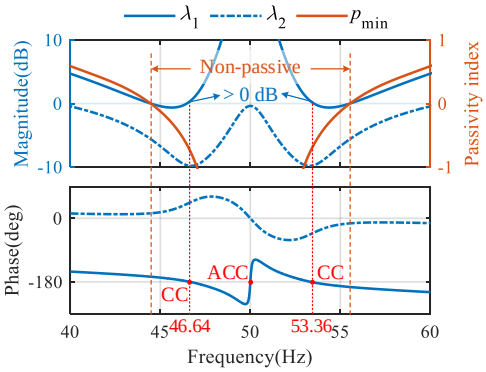

(a)

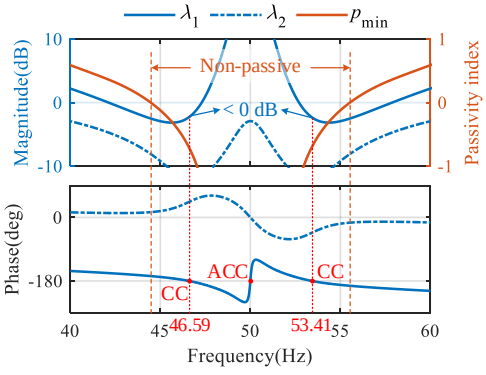

(b)

Figure 4-12 Generalized NSC applied to **L** under different SCRs. (a) SCR=10; (b) SCR=7. Source: [J5].

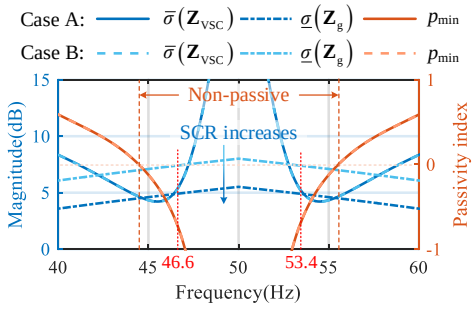

Figure 4-13 Impedance singular value analysis under different SCRs. Source: [J5].

Figure 4-13 shows the singular value analysis of $\mathbf{Z}_{\text{VSC}}$ and $\mathbf{Z}_{\text{g}}$ considering the SCR variation. It is found that as the SCR increases, the frequency range for which

$\bar{\sigma}(\mathbf{Z}_{\mathrm{VSC}}) > \underline{\sigma}(\mathbf{Z}_{\mathrm{g}})$ becomes wider. It is indicated that the frequency range for the eigenvalue of **L** larger than 0 dB also becomes wider. Since the non-passive region of the converter impedance is almost unchanged under the same control parameters and operating conditions, the grid-connected converter system tends to be unstable with higher SCR. This singular value analysis also indicates that the high gain of $\mathbf{Z}_{\mathrm{VSC}}$ at the fundamental frequency poses challenges for the system stability, since it violate the small-gain theorem when the converter is interacting with the grid impedance.

4.2.3.2 Control-Loop Impact Analysis

To futher explain why the converter impedance $\mathbf{Z}_{\mathrm{VSC}}$ has a high gain at the grid fundamental frequency that tends to destabilize the system, the impedance decomposition is applied. According to Figure 4-11(a), the different controller impacts are shaped by $\mathbf{Z}_{\mathrm{o}}$, $\mathbf{G}_{vv}\mathbf{Z}_{\mathrm{refP}}$ and $\mathbf{G}_{vv}\mathbf{Z}_{\mathrm{refQ}}$. They can be compared on Bode diagrams to show the impacts of different control loops, which are given in Figure 4-14. From the magnitude plots of the diagonal elements, it can be seen that the high gain at 50 Hz is mainly caused by the APC, since an integral controller is used in the APC for synchronization. When far from 50 Hz, the VC's impact is dominant, where the APC and RPC's impacts can be neglected. In the frequency range in the red dashed ellipses, there are more stronger interactions among the three control loops, since their magnitudes are closer.

Such magnitude analysis based on decomposed control impedances can provide design guidelines for stability enhancement of grid-forming converters in stiff grids. Since it is already known that the stability in stiff grids is very sensitive to the high gain of $\mathbf{Z}_{\mathrm{VSC}}$ around 50 Hz, if the converter controller tuning can reduce the magnitude of $\mathbf{Z}_{\mathrm{VSC}}$, the system stability can be improved. For the previous case study shown in Figure 4-12, the critical oscillation modes in the $\alpha\beta$ frame are found around 46.6 Hz and 53.4 Hz, which are marked in Figure 4-14. By comparing the magnitudes of VC, APC, and RPC impedances, it is found that the VC and APC are more sensitive to the stability, while RPC is less sensitive.

Three control parameter tuning strategies to reduce the magnitude of $\mathbf{Z}_{\mathrm{VSC}}$ can be chosen as follows:

- By increasing the control bandwidth of VC, the impedance magnitude of $\mathbf{Z}_{\mathrm{o}}$ can be futher decreased around 50 Hz, which benefits to the decrease of the magnitude of $\mathbf{Z}_{\mathrm{VSC}}$.
- By decreasing the APC droop coefficient, the impedance magnitude of $\mathbf{Z}_{\mathrm{refP}}$ can be futher decreased around 50 Hz, which benefits to the decrease of the magnitude of $\mathbf{Z}_{\mathrm{VSC}}$.
- By decreasing the RPC droop coefficient, the impedance magnitude of $\mathbf{Z}_{\mathrm{refQ}}$ can also be futher decreased around 50 Hz. However, this parameter tuning

can hardly make a difference in stability enhancement, since the RPC's impact is much weaker than VC and APC.

Based on the above three control parameter tuning strategies under SCR=10, the stability analysis the the generalized NSC is conducted in Figure 4-15. It can be seen that by tuning VC or APC parameters, the stability is improved significantly compared with Figure Figure 4-12(a). However, changing the RPC parameter almost does not improve the stability. The results verify the previous analysis based on impedance decompostion.

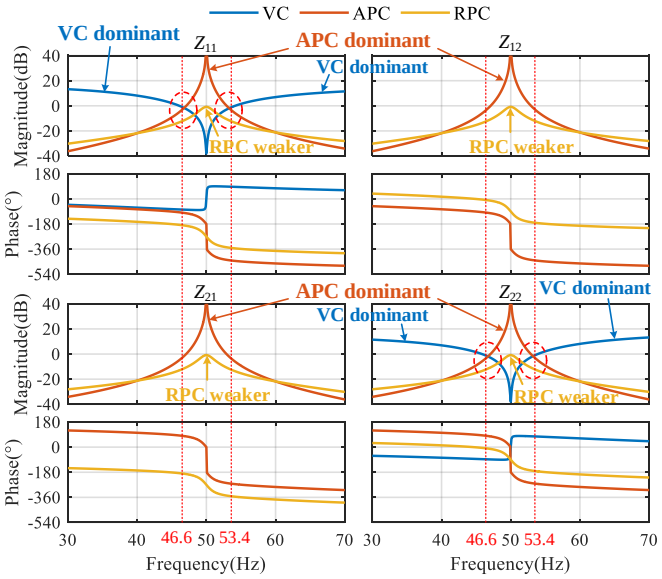

Figure 4-14 Bode diagrams of decomposed control impedances. Source: [J5].

Simulation and experimental results are also provided in Figure 4-16 for validation. Under SCR=10, increasing the VC bandwidth (BW) or decreasing the APC droop coefficient (m_P) can stablize the system, while decreasing the RPC droop coefficient (n_Q) cannot.

It is found from Figure 4-16(c) that the oscillation frequency in the power waveforem is around 3.2 Hz, which becomes 46.8 Hz and 53.2 Hz in the $\alpha\beta$ frame and agrees with the stability analysis result in Figure 4-15(c).

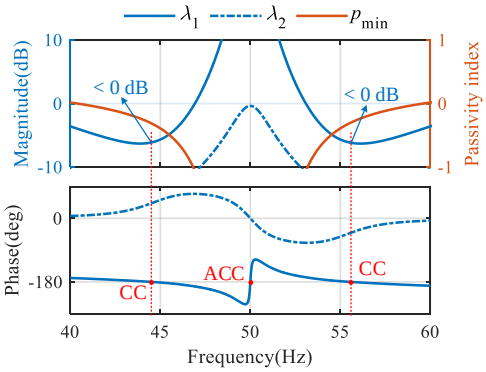

(a)

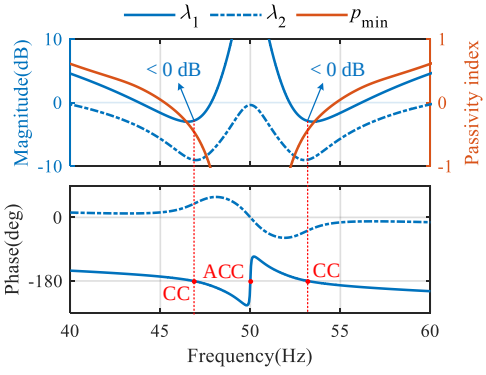

(b)

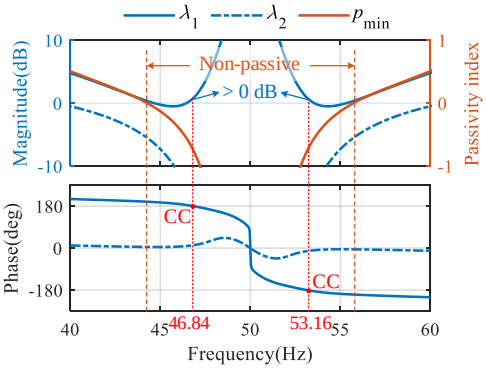

(c)

Figure 4-15 Stability analysis based on design-oriented controller tuning. (a) Reducing VC bandwidth; (b) Reducing APC droop coefficient; (c) Reducing RPC droop coefficient. Source: [J5].

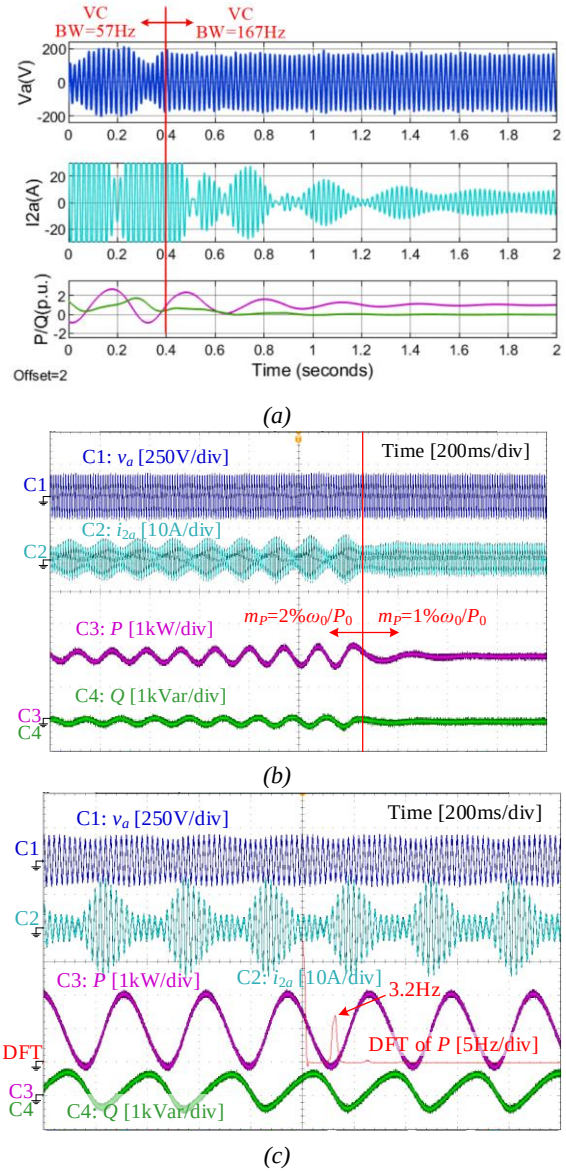

Figure 4-16 Simulation and experimental results based on design-oriented controller tuning. (a) Reducing VC bandwidth; (b) Reducing APC droop coefficient; (c) Reducing RPC droop coefficient. Source: [J5].

4.2.4. SUMMARY

The impedance decomposition approach for the grid-forming converter modeling has been proposed to characterize the impacts of different control loops. Based on the impedance-based stability analysis and the small-gain theorem, it is found that

- The grid-forming converters feature high impedance gain in the low-frequency range, which tends to destabilize the converter system in stiff grids.
- The impedance decomposition approach provides more insights on how each control loop impact the low-frequency high gain of the converter output impedance, which thus benefits to the controller design.

CHAPTER 5. CONCLUSIONS AND PROSPECTS

"Every great and deep difficulty bears in itself its own solution. It forces us to change our thinking in order to find it."

— Niels Bohr

5.1. CONCLUSIONS

This PhD thesis has presented a holistic study on impedance-based modeling, stability analysis and control design for grid-interactive converters. It ranges from the development of fundamental frequency-domain modeling and impedance-based stability analysis approaches, to the application of these approaches to the control design of grid-forming converters. The major conclusions are summarized as follows.

- The existing complex-valued stationary-frame impedance model for three-phase converters can be generalized to unbalanced grid conditions. The frequency-domain model characterizes more frequency-coupling dynamics, which are introduced by the unbalanced voltage trajectory and can be modeled by harmonic transfer functions. Such models can be directly measured in the stationary frame by the proposed frequency scan approach considering the frequency coupling and phase dependence.
- For the impedance-based stability analysis, the "impedance ratio" should be defined as a proper function to ensure the applicability of the NSC. Then, the stability can be directly conducted on Bode diagrams of individual impedances even with the existence of open-loop RHP poles, which enables to implement the impedance specification on Bode diagrams. This approach can be extended to MIMO systems, where MIMO transfer function models can be transformed into equivalent SISO models. Then, the SISO-based stability analysis approaches can still be applied.
- For grid-forming converters, different voltage control schemes (i.e., single-loop and dual-loop control) result in different non-passive regions of converter output impedance. Considering the time delay impact, the virtual impedance control can be co-designed with the voltage controllers, which achieves the impedance passivity till half of the sampling frequency.
- Considering the power-loop control dynamics, the grid-forming converters feature a high impedance at the grid fundamental frequency, which tends to destabilize the system in stiff grids. Through the impedance decomposition based on control loops, it has been found that the integral controller in the active power control loop is the main cause of this high impedance gain at the fundamental frequency. Other controller loops, such as a slow voltage control loop, could also contribute to the high impedance gain in the low-

frequency range and thus affect the stability of grid-forming converters in stiff grids.

5.2. PROSPECTS

Based on the results of the PhD project, some more prospects that are worthy of being investigated in the future are summarized as follows:

- The frequency-domain modeling of converter systems relies on the number of harmonics in the steady-state trajectories. However, these harmonic levels may vary with time and at different locations. How to select the necessary harmonic orders for adequate dynamic representations of power converters needs to be further investigated, which requires using control system theories to perform the model truncation.
- The impedance-based stability analysis merely evaluates the stability at one point of connection. In this thesis, the stability analysis for grid-connected converter systems is mainly focused at converter side in order to investigate the converter-grid interaction. In actual power systems, the grid side may include more complex networks and other converter-based sources and loads. How to apply the impedance-based stability analysis approach in more practical and complex power systems, considering the network partition and model aggregation, could be further investigated.
- The stability analysis for grid-forming converters is simply conducted based a simple grid-connected model, and only a specific control scheme (e.g., droop control with dual-loop voltage control) is studied. In the future, more complex grid models and different grid-forming control schemes (such as with other types of power controls and different virtual impedance controls) can be further investigated. Active damping controllers can also be designed to improve the robustness against grid disturbance.
- Furthermore, future power grid will be based on both SGs and converter-based resources controlled with different schemes, whose proportion keeps varying with the intermittent renewable energy sources. The control interactions among different types of converters as well as SGs can also be studied.
- The existing frequency-domain passivity-based control methods are mainly designed for the frequency range below half of the sampling frequency. There could be still potential for harmonic instability beyond the sampling frequency, which cannot be simply characterized by the averaged model. How to model such systems and design controllers to further widen the passive region beyond the sampling/switching frequency could be further investigated.

BIBLIOGRAPHY

[1] D. Boroyevich, I. Cvetkovic, R. Burgos, and D. Dong, “Intergrid: A future electronic energy network,” IEEE J. Emerg. Sel. Top. Power Electron., vol. 1, no. 3, pp. 127–138, Sep. 2013.

[2] B. Kroposki et al., “Achieving a 100% renewable grid: Operating electric power systems with extremely high levels of variable renewable energy,” IEEE Power Energy Mag., vol. 15, no. 2, pp. 61–73, Mar./Apr. 2017.

[3] F. Blaabjerg, R. Teodorescu, M. Liserre, and A. V. Timbus, “Overview of control and grid synchronization for distributed power generation systems,” IEEE Trans. Ind. Electron., vol. 53, no. 5, pp. 1398–1409, Oct. 2006.

[4] X. Wang and F. Blaabjerg, “Harmonic Stability in Power Electronic Based Power Systems: Concept, Modeling, and Analysis,” IEEE Trans. Smart Grid, vol. 10, no. 3, pp. 2858–2870, May 2019.

[5] X. Wang, M. G. Taul, H. Wu, Y. Liao, F. Blaabjerg and L. Harnefors, "Grid-Synchronization Stability of Converter-Based Resources—An Overview," IEEE O. J. Ind. Appl., vol. 1, pp. 115-134, 2020.

[6] R. W. Erickson, D. Maksimovic, Fundamentals of Power Electronics, Springer Nature Switzerland, 2020.

[7] D. Yang and X. Wang, "Unified Modular State-Space Modeling of Grid-Connected Voltage-Source Converters," IEEE Trans. Power Electron., vol. 35, no. 9, pp. 9700-9715, Sept. 2020.

[8] J. Sun, “Impedance-based stability criterion for grid-connected inverters,” IEEE Trans. Power Electron., vol. 26, no. 11, pp. 3075–3078, Nov. 2011.

[9] G. C. Verghese, I. J. Perezarriaga, and F. C. Schweppe, "Selective modal analysis with applications to electric power systems, part II: the dynamic stability problem," IEEE Trans. Power Apparat. Syst., vol. PAS-101, pp. 3126-3134, Sep. 1982.

[10] X. Wang, F. Blaabjerg, and W. Wu, “Modeling and analysis of harmonic stability in an AC power-electronics-based power system,” IEEE Trans. Power Electron., vol. 29, no. 12, pp. 6421–6432, Dec. 2014.

[11] L. Harnefors, M. Bongiorno and S. Lundberg, "Input-admittance calculation and shaping for controlled voltage-source converters," IEEE Trans. Ind. Electron., vol. 54, no. 6, pp. 3323-3334, Dec. 2007.

[12] B. Wen, D. Boroyevich, R. Burgos, P. Mattavelli, Z. Shen, “Analysis of D-Q small-signal impedance of grid-tied inverters,” IEEE Trans. Power Electron., vol. 31, no. 1, pp. 675–687, Jan. 2016.

[13] J. M. Undrill and T. E. Kostyniak, “Subsynchronous oscillations, part 1 – comprehensive system stability analysis,” IEEE Trans. Power Appar. Syst., vol. PAS–95, no. 4, pp. 1446–1455, Jul./Aug. 1976

[14] R. D. Middlebrook, “Input filter considerations in design and application of switching regulators,” in Proc. IEEE Ind. Appl. Soc. Annu. Meeting, 1976.

[15] Z. Shen, “Online measurement of three-phase AC power system impedance in synchronous coordinates,” Ph.D. dissertation, Dept. of Elect. Eng., Virginia Tech, Blacksburg, USA, 2012.

[16] Y. Liao, Z. Liu, H. Zhang and B. Wen, "Low-Frequency Stability Analysis of Single-Phase System With dq-Frame Impedance Approach—Part I: Impedance Modeling and Verification," IEEE Trans. Ind. Appl., vol. 54, no. 5, pp. 4999-5011, Sept.-Oct. 2018.

[17] H. Gong, X. Wang and D. Yang, "DQ-Frame Impedance Measurement of Three-Phase Converters Using Time-Domain MIMO Parametric Identification," IEEE Trans. Power Electron., vol. 36, no. 2, pp. 2131-2142, Feb. 2021.

[18] C. M. Wildrick, F. C. Lee, B. H. Cho, and B. Choi, “A method of defining the load impedance specification for a stable distributed power system”, IEEE Trans. Power Electron., vol. 10, no. 3, pp. 280–285, May 1995.

[19] L. Harnefors, X. Wang, A. G. Yepes, and F. Blaabjerg, “Passivity based stability assessment of grid-connected VSCs—an overview,” IEEE J. Emerging Sel. Topics Power Electron., vol. 4, no. 1, pp. 116–125, Mar. 2016.

[20] G. W. Wester and R. D. Middlebrook, "Low-frequency characterization of switched dc-dc converters," IEEE Trans. Aero. Electron. Syst., vol. AES-9, pp. 376-385, May 1973.

[21] S. Hiti, D. Boroyevich, and C. Cuadros, “Small-signal modeling and control of three-phase PWM converters,” in Proc. IEEE Ind. Appl. Society Annual Meet., Denver, CO, Oct. 1994, pp. 1143–1150.

[22] L. Harnefors, “Modeling of three-phase dynamic systems using complex transfer functions and transfer matrices,” IEEE Trans. Ind. Electron., vol. 54, no. 4, pp. 2239–2248, Aug. 2007.

[23] Y. Gu, Y. Li, Y. Zhu and T. Green, "Impedance-Based Whole-System Modeling for a Composite Grid via Embedding of Frame Dynamics," IEEE Trans. Power Syst., Early Access, doi: 10.1109/TPWRS.2020.3004377.

[24] A. Rygg, M. Molinas, C. Zhang, and X. Cai, "A modified sequence-domain definition and its equivalence to dq-domain impedance definition for the stability analysis of ac power electronic systems," IEEE J. of Emerg. Sel. Topics Power Electron., vol. 4, no. 4, pp. 1383–1396, Dec. 2016.

[25] C. T. Rim, "Unified General Phasor Transformation for AC Converters," IEEE Trans. Power Electron., vol. 26, no. 9, pp. 2465-2475, Sept. 2011.

[26] L. Harnefors, X. Wang, S. Chou, M. Bongiorno, M. Hinkkanen and M. Routimo, "Asymmetric Complex-Vector Models With Application to VSC–Grid Interaction," IEEE J. Emerg. Sel. Topics Power Electron., vol. 8, no. 2, pp. 1911-1921, Jun. 2020.

[27] X. Wang, L. Harnefors, and F. Blaabjerg, "Unified impedance model of grid-connected voltage-source converters," IEEE Trans. Power Electron., vol. 33, no. 2, pp. 1775–1787, Feb. 2018.

[28] J. Sun and H. Liu, "Sequence impedance modeling of modular multilevel converters," IEEE J. of Emerg. Sel. Topics Power Electron., vol. 5, no. 4, pp. 1427–1443, Dec. 2017.

[29] E. Mollerstedt and B. Bernhardsson, "Out of control because of harmonics – an analysis of the harmonic response of an inverter locomotive," IEEE Control Syst. Mag., vol. 20, no. 4, pp. 70-81, Aug. 2000.

[30] V. Salis, A. Costabeber, S. M. Cox, F. Tardelli, and P. Zanchetta, "Experimental validation of harmonic impedance measurement and LTP Nyquist criterion for stability analysis in power converter networks," IEEE Trans. Power Electron., vol. 34, no. 8, pp. 7972-7982, Aug. 2019.

[31] H. Wu and X. Wang, "Dynamic impact of zero-sequence circulating current on modular multilevel converters: complex-valued AC impedance modeling and analysis," IEEE J. Emerg. Sel. Topics Power Electron., vol. 8, no. 2, pp. 1947-1963, June 2020.

[32] S. Shah and L. Parsa, "Impedance Modeling of Three-Phase Voltage Source Converters in DQ, Sequence, and Phasor Domains," IEEE Trans. Energy Conv., vol. 32, no. 3, pp. 1139-1150, Sept. 2017.

[33] C. Zhang, M. Molinas, A. Rygg, J. Lyu, and X. Cai, "Harmonic transfer function-based impedance modelling of a three-phase VSC for asymmetric AC grids stability analysis," IEEE Trans. Power Electron., vol. 34, no. 12, pp. 12552-12566, Dec. 2019.

[34] A. R. Wood, D. J. Hume, and C. M. Osauskas, "Linear analysis of waveform distortion for HVDC and FACTS devices," in Proc. 9th Int. Conf. on Harmonics and Quality of Power, Orlando, FL, Oct. 2000, pp. 967–972.

[35] A. MacFarlane, "Return-difference and return-ratio matrices and their use in analysis and design of multivariable feedback control systems,"in Proc. Institution Elect. Eng., vol. 117, no. 10, pp. 2037–2049, 1970.

[36] G. F. Franklin, J. D. Powell, and A. Emami-Naeini, Feedback Control of Dynamic Systems, Pearson Education Limited, 2015.

[37] B. Wen, D. Boroyevich, R. Burgos, P. Mattavelli, and Z. Shen, "Inverse Nyquist stability criterion for grid-tied inverters," IEEE Trans. Power Electron., vol. 32, no. 2, pp. 1548–1556, Feb. 2017.

[38] F. Liu, J. Liu, H. Zhang, D. Xue, S. U. Hasan, and L. Zhou, "Stability issues of Z+Z or Y+Y Type Cascade System," in Proc. IEEE Energy Conversion Congress and Exposition (ECCE), 2013, pp. 434-441.

[39] X. Zhang, X. Ruan, and C. K. Tse, "Impedance-based local stability criterion for dc distributed power systems," IEEE Trans. Circuits Syst. I, Fundam. Theory Appl., vol. 62, no. 3, pp. 916–925, Mar. 2015.

[40] X. Feng, J. Liu, and F. C. Lee, "Impedance specifications for stable DC distributed power systems," IEEE Trans. Power Electronics, vol. 17, no. 2, pp. 157-162, 2002.

[41] F. Liu, J. Liu, H. Zhang, and D. Xue, "Stability issues of Z + Z type cascade system in hybrid energy storage system (HESS)," IEEE Trans. Power Electron., vol. 29, no. 11, pp. 5846–5859, Nov. 2014.

[42] H. Liu, X. Xie, X. Gao, H. Liu, and Y. Li, "Stability analysis of SSR in multiple wind farms connected to series-compensated systems using impedance network model", IEEE Trans. Power Syst., vol. 33, no. 3, pp. 3118–3128, May 2018.

[43] B. J. Lurie and P. J. Enright, Classical feedback control with MATLAB and Simulink, Boca Raton, FL, CRC Press, Taylor & Francis Group, 2011.

[44] X. Wang, F. Blaabjerg, and P. C. Loh, “An impedance-based stability analysis method for paralleled voltage source converters”, in Proc. Int. Power Electron. Conf., 2014, pp. 1529-1535.

[45] S. Boyd and L. O. Chua, “On the passivity criterion for LTI N-ports,” Int. J. Circuit Theory and Appl., vol. 10, no. 4, pp. 323–333, Oct. 1982.

[46] L. Harnefors, A. G. Yepes, A. Vidal, and J. Doval-Gandoy, “Passivity-based controller design of grid-connected VSCs for prevention of electrical resonance instability,” IEEE Trans. Ind. Electron., vol. 62, no. 2, pp. 702–710, Feb. 2015.

[47] F. Hans, W. Schumacher, S. Chou, and X. Wang, “Passivation of current-controlled grid-connected VSCs using passivity indices,” IEEE Trans. Ind. Electron., vol. 66, no. 11, pp. 8971–8980, Nov. 2019.

[48] X. Wang, F. Blaabjerg, and P. C. Loh, “Passivity-based stability analysis and damping injection for multiparalleled VSCs with LCL filters,” IEEE Trans. Power Electron., vol. 32, no. 11, pp. 8922–8935, Nov. 2017.

[49] D. Lu, X. Wang, and F. Blaabjerg, “Impedance-based analysis of DC-link voltage dynamics in voltage-source converters,” IEEE Trans. Power Electron., vol. 34, no. 4, pp. 3973–3985, Apr. 2019.

[50] A. J. Agbemuko, J. L. Dominguez-Garcia, O. Gomis-Bellmunt, and L. Harnefors, “Passivity-based analysis and performance enhancement of a vector controlled VSC connected to a weak ac grid,” IEEE Trans. Power Delivery, Early Access, DOI: 10.1109/TPWRD.2020.2982498.

[51] Y. Liao, Z. Liu, H. Zhang and B. Wen, "Low-Frequency Stability Analysis of Single-Phase System With dq-Frame Impedance Approach—Part II: Stability and Frequency Analysis," IEEE Trans. Ind. Appl., vol. 54, no. 5, pp. 5012-5024, Sept.-Oct. 2018.

[52] J. Rocabert, A. Luna, F. Blaabjerg, and P. Rodriguez, “Control of power converters in AC microgrids,” IEEE Trans. Power Electron., vol. 27, no. 11, pp. 4734–4749, Nov. 2012.

[53] L. Zhang, L. Harnefors, and H. Nee, “Power-synchronization control of grid-connected voltage-source converters,” IEEE Trans. Power Syst., vol. 25, no. 2, pp. 809–820, May 2010.

[54] L. Zhang, L. Harnefors, and H. Nee, “Interconnection of two very weak AC systems by VSC-HVDC links using power-synchronization control,” IEEE Trans. Power Syst., vol. 26, no. 1, pp. 344–355, Feb. 2011.

[55] P. Mitra, L. Zhang, and L. Harnefors, “Offshore wind integration to a weak grid by VSC-HVDC links using power-synchronization control: a case study,” IEEE Trans. Power Del., vol. 29, no. 1, pp. 453–461, Feb. 2014.

[56] J. Khazaei, Z. Miao, and L. Piyasinghe, “Impedance-model-based MIMO analysis of power synchronization control,” Electric Power Systems Research, vol. 154, pp. 341–351, Jan. 2018.

[57] L. Huang, H. Xin, and Z. Wang, “Damping low-frequency oscillations through VSC-HVDC stations operated as virtual synchronous machines,” IEEE Trans. Power Electron., vol. 34, no. 6, pp. 5803–5818, Jun. 2019.

[58] G. Denis, T. Prevost, P. Panciatici, X. Kestelyn, F. Colas, and X. Guillaud, “Improving robustness against grid stiffness, with internal control of an AC voltage-controlled VSC.,” in Proc. IEEE Power and Energy Society General Meeting (PESGM), Boston, MA, Nov. 2016.

[59] T. Qoria, F. Gruson, F. Colas, X. Kestelyn, X. Guillaud, “Analysis of the coupling between the outer and inner control loops of a Grid-forming Voltage Source Converter,” in Proc. Europ. Conf. Power Electron. and Appl. (EPE), Sep. 2020.

[60] S. D’Arco, J. A. Suul, and O. Fosso, “Automatic tuning of cascaded controllers for power converters using eigenvalue parametric sensitivities,” IEEE Trans. Ind. Appl., vol. 51, no. 2, pp. 1743–1753, Mar. – Apr. 2015.

[61] S. Wang, Z. Liu, J. Liu, D. Boroyevich, and R. Burgos, “Small-signal modeling and stability prediction of parallel droop-controlled inverters based on terminal characteristics of individual inverters,” IEEE Trans. Power Electron., vol. 35, no. 1, pp. 1045-1063, Jan. 2020.

[62] W. Cao, Y. Ma, F. Wang, L. M. Tolbert, and Y. Xue, “Low-frequency stability analysis of inverter-based islanded multiple-bus AC microgrids based on terminal characteristics”, IEEE Trans. Smart Grid, vol. 11, no. 5, pp. 3662-3676, Sept. 2020.

[63] X. Yue, X. Wang, and F. Blaabjerg, “Review of small-signal modeling methods including frequency-coupling dynamics of power converters,” IEEE Trans. Power Electron., vol. 34, no. 4, pp. 3313–3328, Apr. 2019.

[64] J. Groves, "Small-signal analysis using harmonic balance methods," in Proc. IEEE Power Electron. Spec. Annual Conf. (PESC), Cambridge, MA, USA, 1991, pp. 74-79.

[65] A. Packard, K. Poolla, and R. Horowitz, “Dynamic systems and feedback class notes,” Dept. Mech. Eng., Univ. California, Berkeley, CA, USA, Spring 2005.

[66] N. M. Wereley, “Analysis and control of linear periodically time varying systems,” Ph.D. dissertation, Dept. of Aeronautics and Astronautics, MIT, 1991.

[67] W. Ren and E. Larsen, “A refined frequency scan approach to sub-synchronous control interaction (SSCI) study of wind farms,” IEEE Trans. Power Syst., vol. 31, no. 5, pp. 3904–3912, Sep. 2016.

[68] A. M. Stankovic and T. Aydin, “Analysis of unbalanced power system faults using dynamic phasors,” IEEE Trans. Power Syst., vol. 15, no. 3, pp. 1062-1068, Aug. 2000.

[69] A. M. Stankovic, S. R. Sanders, and G. C. Verghese, “Dynamic phasors in modeling and analysis of unbalanced polyphaser ac machines,” IEEE Trans. Energy Conv., vol. 17, no. 1, pp. 107-113, Mar. 2002.

[70] P. Stefanov and A. M. Stankovic, “Modeling of UPFC operation under unbalanced conditions with dynamic phasors,” IEEE Trans. Power Syst., vol. 17, no. 2, pp. 395-403, May 2002.

[71] Y. Liao, X. Wang, X. Yue, and H. Gong, “Harmonic transfer-function model of three-phase synchronous reference frame PLL under unbalanced grid conditions,” in Proc. IEEE Appl. Power Electron. Conf. (APEC), Anaheim, CA, Mar. 2019, pp. 58–65.

[72] H. Nyquist, “Regeneration theory,” Bell Syst. Tech. Journ., vol. 11, no. 1, pp. 126–147, Jan. 1932.

[73] D. Lumbreras, E. L. Barrios, A. Urtasun, A. Ursúa, L. Marroyo, and P. Sanchis, “On the stability of advanced power electronic converters: the generalized Bode criterion,” IEEE Trans. Power Electron., vol. 34, no. 9, pp. 9247–9262, Sep. 2019.

[74] G. C. Paap, “Symmetrical components in the time domain and their application to power network calculations,” IEEE Trans. Power Syst., vol. 15, no. 2, pp. 522-528, May. 2000.

[75] Z. Li, Y. Li, P. Wang, H. Zhu, C. Liu, and F. Gao, “Single-loop digital control of high-power 400-Hz ground power unit for airplanes,” IEEE Trans. Ind. Electron., vol. 57, no. 2, pp. 532–543, Feb. 2010.

[76] X. Wang, P. C. Loh, and F. Blaabjerg, “Stability analysis and controller synthesis for single-loop voltage-controlled VSIs,” IEEE Trans. Power Electron., vol. 32, no. 9, pp. 7394–7404, Sep. 2017.

[77] M. J. Ryan, W. E. Brumsickle, and R. D. Lorenz, “Control topology options for single-phase UPS inverters,” IEEE Trans. Ind. Appl., vol. 33, no. 2, pp. 493–501, Mar./Apr. 1997.

[78] P. C. Loh and D. G. Holmes, “Analysis of multiloop control strategies for LC/CL/LCL-filtered voltage-source and current-source inverters,” IEEE Trans. Ind. Appl., vol. 41, no. 2, pp. 644–654, Mar./Apr. 2005.

[79] Y. W. Li, “Control and resonance damping of voltage-source and current source converters with LC filters,” IEEE Trans. Ind. Electron., vol. 56, no. 5, pp. 1511–1521, May 2009.

[80] F. Bosio, L. A. S. Ribeiro, F. D. Freijedo, M. Pastorelli, and J. M. Guerrero, “Effect of state feedback coupling and system delays on the transient performance of stand-alone VSI with LC output filter,” IEEE Trans. Ind. Electron., vol. 63, no. 8, pp. 4909 – 4918, Aug. 2016.

[81] M. A. Awal, W. Yu, and I. Husain, “Passivity Based Predictive-Resonant Current Control for Resonance Damping in LCL-Equipped VSCs,” IEEE Trans. Ind. Appl., Early access, DOI: 10.1109/TIA.2019.2959594.

[82] H. Bai, X. Wang, and F. Blaabjerg, “Passivity enhancement in renewable energy source based power plant with paralleled grid-connected VSIs,” IEEE Trans. Ind. Appl., vol. 53, no. 4, pp. 3793–3802, Jul./Aug. 2017.

[83] H. Yu, M. A. Awal, H. Tu, Y. Du, S. Lukic, and I. Husain, “Passivity-oriented discrete-time voltage controller design for grid-forming inverters,” in Proc. IEEE Energy Conversion Congress and Exposition (ECCE), Baltimore, MD, USA, Sep. 2019, pp. 469–475.

[84] Y. Liao and X. Wang, “Passivity analysis and enhancement of voltage control for voltage-source converters,” in Proc. IEEE Energy Conversion Congress and Exposition (ECCE), Baltimore, MD, USA, Sep. 2019, pp. 5424–5429.

[85] Y. Liao and X. Wang, “Evaluation of voltage regulators for dual-loop control of voltage-controlled VSCs,” in Proc. IEEE Energy Conversion Congress and Exposition (ECCE), Baltimore, MD, USA, Sep. 2019, pp. 5036–5042.

[86] Y. Liao, X. Wang, F. Liu, K. Xin and Y. Liu, "Sub-Synchronous Control Interaction in Grid-Forming VSCs with Droop Control," in Proc. IEEE

Workshop on the Electronic Grid (eGRID), Xiamen, China, Nov. 2019, pp. 1-6.

[87] J. Bao, F. Wang, P. L. Lee, and W. Zhou, “New frequency-domain phase-related properties of MIMO LTI passive systems and robust controller synthesis,” in Proc. 13th World Congr of IFAC, San Francisco, USA, Jun.-Jul. 1996, pp. 3276-3281.

APPENDED PUBLICATIONS

[J1] **Yicheng Liao** and Xiongfei Wang, "Stationary-Frame Complex-Valued Frequency-Domain Modeling of Three-Phase Power Converters," ***IEEE Journal of Emerging and Selected Topics in Power Electron*ics**, vol. 8, no. 2, pp. 1922-1933, Jun. 2020.

[J2] **Yicheng Liao**, Xiongfei Wang, Xiaolong Yue, and Lennart Harnefors, "Complex-Valued Multi-Frequency Admittance Model of Three-Phase VSCs in Unbalanced Grids," ***IEEE Journal of Emerging and Selected Topics in Power Electron*ics**, vol. 8, no. 2, pp. 1934-1946, Jun. 2020.

[J3] **Yicheng Liao** and Xiongfei Wang, "Impedance-Based Stability Analysis for Interconnected Converter Systems with Open-Loop RHP Poles," ***IEEE Transactions on Power Electron*ics**, vol. 35, no. 4, pp. 4388-4397, Apr. 2020.

[J4] **Yicheng Liao**, Xiongfei Wang, and Frede Blaabjerg, "Passivity-Based Analysis and Design of Linear Voltage Controllers For Voltage-Source Converters," ***IEEE Open Journal of the Industrial Electronics Society***, vol. 1, pp. 114-126, 2020.

[J5] **Yicheng Liao** and Xiongfei Wang, "Impedance Decomposition for Design-Oriented Analysis of Grid-Forming Voltage-Source Converters," ***IEEE TechRxiv***, Aug. 2020, DOI: 10.36227/techrxiv.12855167.

ISSN (online): 2446-1636
ISBN (online): 978-87-7210-865-0 AALBORG UNIVERSITY PRESS